ELSEVIER

Sedimentary Geology 124 (1999) 81–111

Sedimentary Geology

Provenance of Cretaceous synorogenic sandstones in the Eastern Alps: constraints from framework petrography, heavy mineral analysis and mineral chemistry

Hilmar von Eynatten *, Reinhard Gaupp

Institut für Geowissenschaften, Friedrich-Schiller-Universität Jena, Burgweg 11, D-07749 Jena, Germany

Received 1 November 1997; accepted 14 July 1998

Abstract

The detrital components of Cretaceous sedimentary rocks in the Northern Calcareous Alps reflect the early Alpine geodynamic evolution of the Austroalpine microplate. Two contrasting source areas are distinguished on the base of light and heavy mineral analysis. The first source area is located at the southeastern margin of the Austroalpine and is composed of Palaeozoic sediments and metamorphic rocks, Mesozoic carbonate rocks, and ultrabasic rocks derived from the suture zone of the Vardar/Meliata Ocean. The second source area is located in the northwest in a Lower Austroalpine position near the transpressive plate margin that juxtaposes Austroalpine and Penninic units. This source area comprises Palaeozoic low-grade metamorphic rocks including high-pressure (HP) rocks, late Palaeozoic (meta)sediments, Mesozoic carbonate rocks, and ultrabasic rocks from obducted slices of Penninic oceanic crust. Chemical analyses of detrital white mica, amphibole and garnet support the discrimination between the two source areas. Tourmaline chemistry calls for a significant amount of metasedimentary rocks in the source area. Granitoid rocks and high-grade metamorphic rocks are rare. Blue amphibole, phengite, and chloritoid composition suggest the erosion of lower blueschist facies rocks in the northwestern source area. We suggest a modified model of Austroalpine Valanginian to Coniacian tectono-sedimentary evolution which is based on (1) an onset of subduction of the Penninic Ocean no earlier than Late Cretaceous, (2) deposition of the analyzed sedimentary rocks in piggyback basins, and (3) a reconstruction of provenance as proposed in this study.

Keywords: sandstone; petrography; heavy minerals; provenance; Cretaceous; Eastern Alps

1. Introduction

Provenance analysis serves to reconstruct the predepositional history of a sediment or sedimentary rock. This includes the distance and direction of transport, size and setting of the source region, climate and relief in the source area, and the specific types of source rocks (Pettijohn et al., 1987). Geological information on ancient earth surfaces (potential source areas) is crucial for understanding the geological history and geodynamic processes through space and time. This is certainly the case when the source areas were removed due to erosion, tectonism, or burial by younger sediments (e.g., former mountain belts; Ibbeken and Schleyer, 1991). In the Eastern Alps, Cretaceous source areas were com-

* Corresponding author.

0037-0738/99/$ – see front matter
PII: S0037-0738(98)00122-5

plex and included two oceanic suture zones. They were eroded and/or tectonically displaced during the later Tertiary orogeny. Therefore, the Cretaceous sedimentary rocks are important witnesses of the early Alpine evolution (e.g., Gaupp, 1982; Faupl and Wagreich, 1992).

The aim of this paper is to reconstruct the provenance of Cretaceous (Valanginian to Santonian) synorogenic sandstones of the Eastern Alps. The study is carried out using an integrated approach of several analytical techniques. Light mineral analysis is used to restrict the range of possible source rocks to a few major rock types and to derive a semi-quantitative weathering index for these sediments (cf. Grantham and Velbel, 1988). Heavy mineral analysis is a very effective tool for provenance discrimination (Ibbeken and Schleyer, 1991). Chemical analyses of several detrital mineral phases serve to constrain source rock petrology and to emphasize discrimination between different source areas (Morton, 1991). The data are used to establish a tectono-sedimentary model of the Cretaceous evolution of the Eastern Alps. The model is supported by geochronological data which allow us to assess the cooling ages of specific detrital mineral phases (von Eynatten et al., 1996, 1997a).

2. Geological setting and palaeogeography

The analyzed Cretaceous sedimentary rocks belong to the Northern Calcareous Alps (NCA, Fig. 1). The NCA form the northernmost part of the Austroalpine continental crustal unit which is located at the northern tip of the Adriatic plate. The Adriatic plate was separated from the European plate by the opening of the Penninic (Piemontais) Ocean in the Middle Jurassic (Fig. 2). The opening of the Penninic Ocean was directly linked to the initial opening of the Atlantic Ocean by a sinistral transform zone (e.g., Dewey et al., 1973; Channell and Horwath, 1976; Frisch, 1979). A second oceanic realm was located to the east of the Adriatic plate. This western branch of the Tethys Ocean (Vardar and/or Meliata Ocean, Fig. 2) was closed in the Late Jurassic. As a consequence, the style of plate tectonics changed in the Alpine region resulting in a dextral transpressive movement of the Austroalpine microplate relative to stable Europe (e.g., Faupl and Wagreich, 1992). This

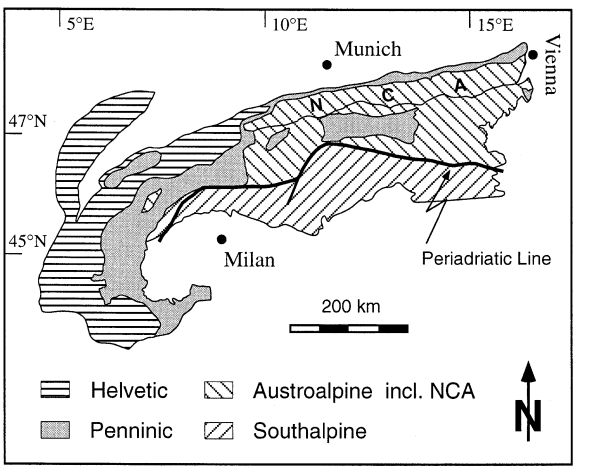

Fig. 1. Simple geological–structural sketch of the Alpine arc showing location of the Northern Calcareous Alps (NCA) as the northernmost part of the Austroalpine unit.

led to the final closure of the Penninic Ocean in the Eocene.

Based on palaeomagnetic and structural data the Austroalpine microplate was decoupled from the Adriatic plate (including the Southalpine unit, Fig. 2) during Jurassic/Cretaceous time (Neubauer, 1987; Channell et al., 1992). The final closure of the Vardar/Meliata Ocean led to the formation of an initial nappe pile at the southeastern margin of the Austroalpine microplate which included the Vardar/Meliata oceanic suture zone (Neubauer, 1994; Froitzheim et al., 1996). From this nappe pile sediments started to be shed into the Austroalpine realm in the ?Berriasian/Valanginian (Faupl and Tollmann, 1979; Darga and Weidich, 1986). At the northwestern rim of the Austroalpine microplate (the former passive margin to the Penninic Ocean) compressive movements led to the formation of an antiform ('North-Adriatic obduction belt', cf. Winkler, 1996) that experienced erosion from the Aptian/Albian onward. The sediments were shed to the southeast into the Austroalpine realm (Gaupp, 1982, 1983).

The NCA are composed of a complex, presently east–west elongated, nappe pile mostly consisting of Mesozoic carbonate rocks. This nappe pile was detached from its original crystalline basement during the Late Cretaceous. Subsequently, the NCA were thrust over Penninic oceanic crustal units and European continental crustal units (Helvetic, Fig. 1).

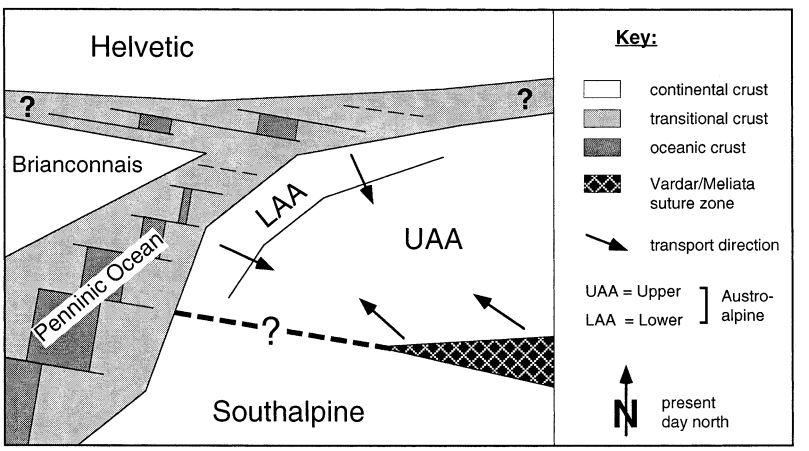

Fig. 2. Palaeogeographic sketch of the Alpine realm at the Jurassic/Cretaceous boundary (approx. 145 Ma; Harland et al., 1990; see Fig. 3). Arrows indicate transport directions of the later Cretaceous sediments into the depositional area of the Upper Austroalpine (modified from Pober and Faupl, 1988; Faupl and Wagreich, 1992).

Deposition of the studied Cretaceous sedimentary rocks was contemporary with the formation of the nappe pile of the NCA. The stratigraphic age of the youngest of these siliciclastic rocks in each nappe is used to assess the age of thrusting of the next higher nappe (Gaupp, 1982). Postdepositional crustal shortening and ongoing thrusting caused intensive deformation and folding of the sediments. The tectonic and thermal overprint increases from northwest to southeast. Vitrinite reflectance and illite crystallinity data show that temperatures during the burial stage of the sediments did not exceed 150 to 200ºC (Gaupp and Batten, 1985; Krumm et al., 1988).

3. Stratigraphy and sedimentology

The analyzed siliciclastic rocks concordantly overlie Upper Jurassic to Lower Cretaceous pelagic limestones (Aptychus Limestone Formation). They are subdivided into four sedimentary successions (Fig. 3); for sample sites and structural position of individual nappes see Fig. 4.

(1) The Rossfeld Formation (RF) ranges stratigraphically from ?Berriasian/Valanginian to Lower Aptian and is restricted to the middle and eastern parts of the NCA and to higher tectonic (mostly Tirolic) nappes (Fig. 4; Faupl and Tollmann, 1979; Darga and Weidich, 1986). The marls, shales, sandstones, and breccias of the RF were deposited within a submarine slope/trench system which developed parallel and in front of the prograding thrust front. The sand-sized material displays features characteristic of turbidites and contourites. Breccias and olistoliths were directly derived from local fault scarps within the nappe front. The detrital material of the RF is derived from a source area in the SE of the Austroalpine which includes the Vardar/Meliata suture zone (Fig. 2; Decker et al., 1987; Pober and Faupl, 1988).

(2) The Lech Formation (LF; former 'Lechtaler Kreideschiefer'; Huckriede, 1958) is restricted to the Lechtal nappe which is located in an intermediate tectonic position within the NCA nappe pile (Fig. 4): structurally lower than the position of the RF sediments, but structurally higher than the position of TLF sediments. Biostratigraphic data indicate an Aptian to Upper Albian/?Cenomanian range for the LF (Winkler, 1988; von Eynatten, 1996). Lithotypes comprise marls, shales, micritic and crinoidal limestones, calclithites (cf. Garzanti, 1991), litharenites, and breccias. The coarse-grained lithotypes (sandstones, breccias) show evidence for deposition by sediment gravity flows. The provenance of the siliciclastic material of the LF is unknown (e.g., Winkler, 1988), but we will show in this paper that a southeastern source area comparable to that of the RF is most probable.

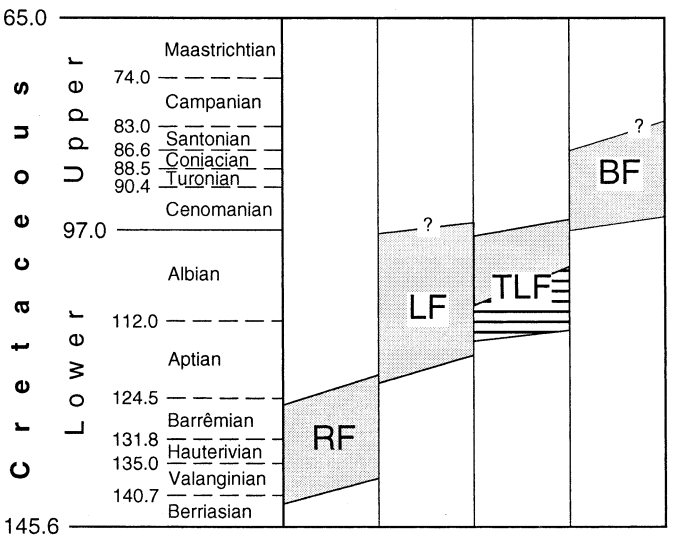

Fig. 3. Schematic sketch of the biostratigraphic range of the analyzed sedimentary successions. Time scale after Harland et al. (1990). All absolute ages in the paper refer to this time scale. *RF* = Rossfeld Formation, *LF* = Lech Formation, *TLF* = Tannheim (line pattern) and Losenstein Formations, *BF* = Branderfleck Formation.

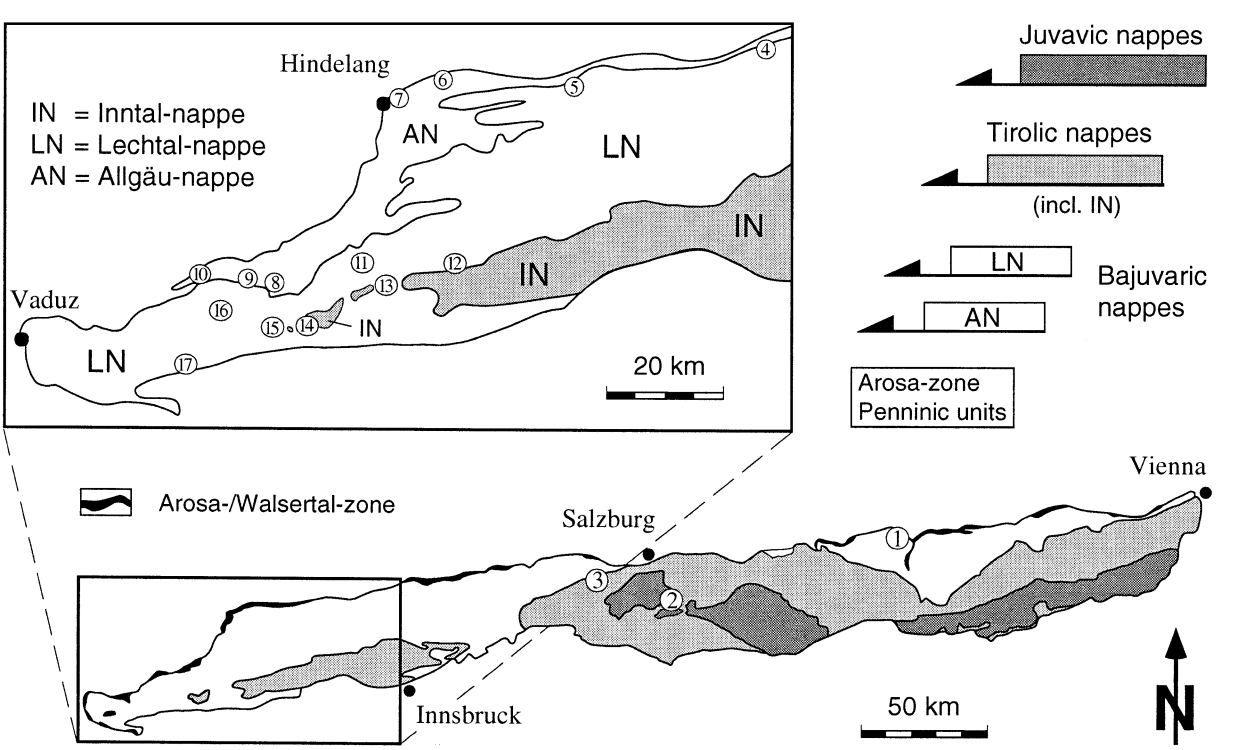

Fig. 4. Simplified structural map of the Northern Calcareous Alps showing areal extent and structural position of the major nappes. Numbers indicate sample localities: *1* = Losenstein, *2* = Rossfeld, *3* = Lackbach, *4* = Wetzstein-Laine *5* = Branderfleck, *6* = Pfarrwiesbach, *7* = Hindelang (Krähenwand, Kleebach, Häusellochbach), *8* = Mohnenfluh area, *9* = Hochberg, *10* = Steristobel, *11* = Holzgau, *12* = Griesbachalm, *13* = Madau, *14* = Trittalm, *15* = Zürser See/Madlochspitze, *16* = Rote Wand, *17* = Lorüns.

(3) The Tannheim and Losenstein Formations (TLF) are restricted to the northernmost and structurally deepest nappe of the NCA (Allgäu nappe, Fig. 4). The Tannheim Formation is composed of marls and marly shales of late Aptian to Albian age (Zacher, 1966). These pelitic sediments grade upsection into a coarser-grained series of shales, sandstones, pebbly mudstones, and conglomerates that were in part deposited by sediment gravity flows (Losenstein Formation). This formation ranges up to the uppermost Albian (Löcsei, 1974; Gaupp, 1982). The transition from the Tannheim Formation to the Losenstein Formation is diachronous within the Albian. The various lithofacies-types of the TLF are interpreted to reflect deposition within a prograding submarine fan system. Facies distribution and clast composition suggest that the source area was located within a Lower Austroalpine (LAA, Fig. 2) to South Penninic position northwestward of the NCA (Gaupp, 1983).

(4) The sedimentary rocks of the Branderfleck Formation (BF) are restricted to the northernmost parts of the Allgäu nappe as well as the Lechtal nappe (Fig. 4; Gaupp, 1982). The oldest sedimentary rocks of the BF are Cenomanian shallow marine marls and calclithites as well as breccias and olistostromes composed of Mesozoic carbonate material. The latter is derived from local fault scarps within the front of the thrust nappes. From the Turonian up to the Coniacian/?Santonian the siliciclastic detritus increases again (Weidich, 1985; Winkler, 1988). Pelitic rocks with intercalations of sandy turbidites dominate the upper part of the BF but intercalations of coarse breccias and olistostromes are present. The provenance of the siliciclastic material of the BF has been controversial in the past (e.g., Gaupp, 1982; Weidich, 1984). In this paper we suggest a northwestern source area comparable to that of the TLF.

4. Methods

4.1. Sandstone framework petrography (light mineral analysis)

Light mineral analysis was performed by point counting of usually 300 framework grains per sample. Thin sections were stained with Alizarin red S to better distinguish calcitic and dolomitic carbonate grains. Cement and (pseudo)matrix were not counted (Dickinson, 1970). Errors were estimated from repeated measurements ($n = 5$) of three thin sections (von Eynatten, 1996) and correspond to those given by van der Plas and Tobi (1965). In contrast to the Gazzi–Dickinson (GD) method (e.g., Zuffa, 1985) minerals or crystals >63 μm within rock fragments were not counted as monomineralic grains but as the type of lithoclast they occur in (e.g., Decker and Helmold, 1985). This is useful because otherwise the sometimes high amounts of ultrabasic and metamorphic detritus would become obscured. Indeed, following the classic GD method, a significant amount of the ultrabasic serpentinite clasts would be assigned to the group of opaque minerals because of their frequent inclusions of Fe-oxides. Further examples are polycrystalline quartz and quartz–mica–chlorite aggregates which in several cases would be assigned to the monoquartz group neglecting the metamorphic origin of these grains. To distinguish between monomineralic grains and lithoclasts (rock fragments) we use the 0% cut-off proposed by Ingersoll et al. (1984).

Our approach better accounts for the variety of lithoclast types, especially in coarse-grained synorogenic deposits with low weathering indices (see Section 5.3). Because sandstone composition depends on sample grain size, the applied counting method may be problematic with regard to the comparison of samples of different grain size (Ingersoll et al., 1984). However, even the classic GD method is not truly independent of grain size (e.g., Bangs Rooney and Basu, 1994). Therefore we focus on a maximum source rock information (that is, the variety of lithoclast types) and the problem of grain size is minimized by sampling a range of sandstones of different grain sizes from each sandstone sedimentary succession.

4.2. Heavy mineral analysis

Weathered rims were removed and the fresh sample material was crushed to small pieces (1 to 4 mm). Disaggregation in warm 10% acetic acid (60 to 70ºC) was enhanced by adding small quantities of H_2O_2 to avoid acetate precipitation (Winkler, 1988), and repeated ultrasonic cleaning to remove

clay mineral coatings, cement, and/or pseudomatrix. The disintegrated and washed sand was separated into several grain size fractions by standardized dry sieving. Heavy minerals were separated by gravity settling in tribromoethane and grain separates were embedded in Meltmount 1.582 (Mange and Maurer, 1991). All heavy mineral data presented in this study were obtained from the 63–125-μm grain size fraction for two reasons: (1) analysis of narrow grain size intervals at the fine-grained sand level avoids bias by inherited grain size distributions of the parent rocks (Morton and Hallsworth, 1994), and (2) tests of several samples indicate that the 63–125-μm grain size fraction is the one with the highest heavy mineral concentration independent of the framework grain size of the sample (von Eynatten, 1996). Usually 200 non-opaque non-micaceous grains were counted per sample using the ribbon counting method (Morton, 1985; Mange and Maurer, 1991). Errors were estimated from repeated measurements ($n = 3$ to 5) of four heavy mineral separates (von Eynatten, 1996). They are significantly lower than those given by van der Plas and Tobi (1965).

4.3. Electron microprobe analysis

Heavy minerals for microprobe analysis were handpicked under the microscope. White micas were concentrated from the light mineral fraction by a vibrating inclined plane and subsequent handpicking. Microprobe analyses were carried out with a Cameca Camebax electron microprobe using the wave-length dispersive method, 15 kV acceleration potential, and a beam current of 12 nA. Mineral standards as well as synthetic oxides (Cr_2O_3, MgO, $MnTiO_3$, NiO) were used for calibration. Data were corrected online using standard correction procedures (Pouchou and Pichoir, 1984). Ten elements were analyzed (Si, Ti, Cr, Al, Fe, Mn, Mg, Ca, Na, K) from all mineral phases except for tourmaline (nine elements, no Cr). Fe_2O_3, B_2O_3, and H_2O were calculated assuming mineral stoichiometry. Errors are estimated from Poisson counting statistics and repeated measurements ($n = 6$ to 10) of the same area of an individual grain. Errors are usually less than 1% (1s standard deviation). For low concentrations and/or specific elements in specific phases errors are slightly higher, e.g., 1.8% for Na_2O in blue sodic amphibole, 2.5% for MgO in phengite, and up to 4.3% for FeO in tourmaline (von Eynatten, 1996). Micas were measured in an orientation perpendicular to their crystallographic *c*-axis in order to integrate over several individual sheet layers.

5. Sandstone framework petrography

5.1. Classification and general description

Following the first-level classification of arenites introduced by Zuffa (1980) the analyzed arenitic rocks are sandstones (Fig. 5A). They are almost entirely composed of carbonate and non-carbonate extrabasinal grains (CE and NCE, respectively). Some samples show small amounts ($\ll$10%) of non-carbonate intrabasinal grains (NCI), e.g., rip-up clasts and green glauconitic grains (Garzanti, 1991). As a second-level classification of the sandstones we use the QFL diagram proposed by McBride (1963) with the modification that CE grains are included into the L-pole. This modification is necessary due to the sometimes high content of CE grains because otherwise a sample composed of, e.g., 60% quartzose grains and 40% carbonate grains would be classified as quartzarenite. The light mineral (LM) point-count data of 88 samples define all but one as litharenite (Fig. 5B). Feldspar concentrations are low (usually 1 to 4%, max. 9%).

The litharenites generally display low degrees of roundness and sorting. Clay minerals and/or other matrix-sized material mostly exceed 5% and is generally thought to be of secondary origin (pseudomatrix, Dickinson, 1970; see also Cox and Lowe, 1996). Litharenite components cover a wide range from monomineralic grains (quartz, feldspar, mica, chlorite) to silica/silicate lithoclasts (e.g., polycrystalline quartz, chert, serpentinite, quartz–chlorite–mica aggregates) and carbonate lithoclasts (dolomite, micritic calcite, sparitic calcite). The porosity and permeability of these immature litharenites is negligible. Cements are rare and if present mostly calcite. Features like concavo–convex grain contacts, deformed micas, and squeezing of soft lithoclasts are common and reflect the postdepositional tectonothermal overprint (see Section 2).

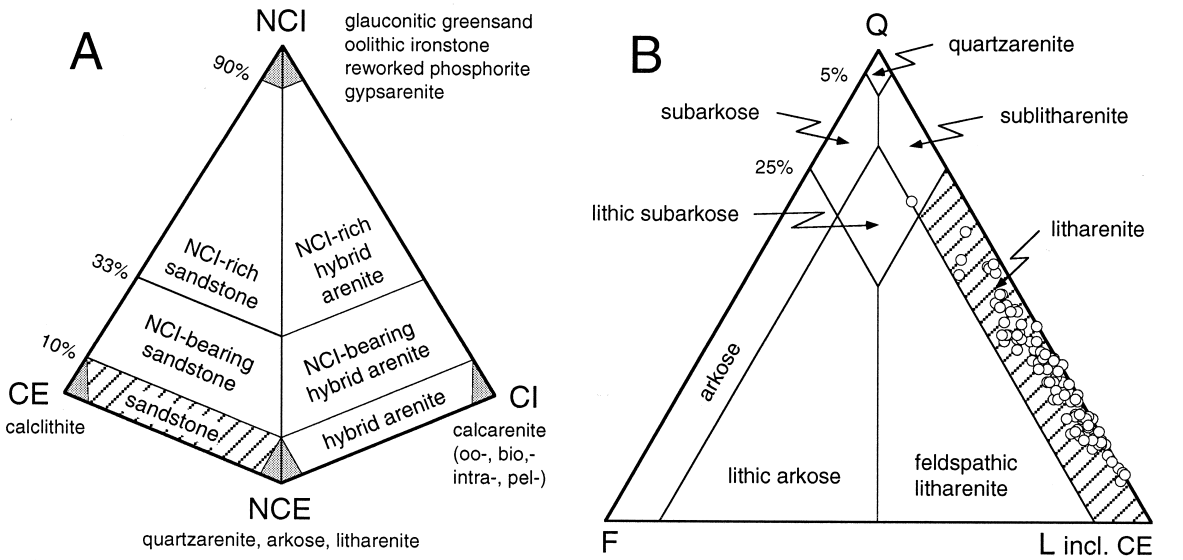

Fig. 5. Classification of the analyzed arenitic rocks based on light mineral data: (A) the first level classification scheme suggested by Zuffa (1980) and (B) the QFL diagram introduced by McBride (1963). All but one of the analyzed sandstones ($n = 88$) are litharenites (see text). For data see Table 1.

5.2. Framework grains and provenance discrimination

The framework grain point-count data (Table 1) suggest a dominance of metamorphic relative to magmatic source rocks due to the low feldspar concentrations (F, see Section 5.1). This observation is supported by the generally low concentration of volcanogenic lithoclasts (L_v, usually 0.0–2.0%, max. 6.0%). In addition, CE-clasts require a carbonate source rock component and serpentinite clasts (L_u) require an ultramafic source rock component. Monocrystalline quartz grains (Q_m) may either originate from metamorphic source rocks or from the recycling of older sedimentary rocks. Characteristic volcanic quartz grains (cf. Folk, 1980) are rare.

Provenance diagrams with respect to the plate tectonic setting of the source area usually disregard carbonate clasts (e.g., Dickinson and Suczek, 1979; Dickinson, 1985). This may lead to an incorrect interpretation of the tectonic setting (Mack, 1984; Arribas and Arribas, 1991). If CE-clasts are included into the L-pole, the Q_mFL_t diagram is more suitable because in the QFL diagram of Dickinson (1985) high contents of CE-clast lead to the misinterpretation of an undissected and/or transitional arc provenance (von Eynatten, 1996). Fig. 6 shows the framework composition of the sandstones within the Q_mFL_t diagram. The compositional data of all but one sample suggest a recycled orogen provenance of the sediments. The samples plot into the subcategories 'lithic recycled' or 'lithic recycled + transitional recycled', depending whether CE-clasts are included into the L-pole or not.

The framework composition of sandstones from the four sedimentary successions (see Section 3) cannot be sufficiently discriminated using a simple ternary QFL (or Q_mFL_t) diagram (Fig. 7). The only visible trends are (1) a shift towards the L-pole for an average BF sample relative to an average TLF sample, and (2) an average feldspar content of LF samples which is slightly higher in comparison to the other successions. If a discrimination based on light minerals is required the major lithoclast types have to be considered. These are polycrystalline quartz grains (Q_p), quartz–chlorite–mica aggregates (L_{sm}), serpentinite clasts (L_u), as well as dolomitic (D) and calcitic (C_m and C_s) CE-clasts (Table 1). Four classes of light mineral grains were chosen because (a) they make significant proportions of the framework grain spectra of the sandstones, and (b) are closely related to specific source rocks:

Table 1
Light and heavy mineral data of the analyzed samples ($n = 88$) and index of mineral chemistry data

Sample No.	Loc. No.	Sed. Succ.	Light mineral data																
			Q_m	Q_p	Q_c	F	L_{sm}	L_u	L_v	C_m	C_s	D	Others	Q	L	L_t	CE	L + CE	M	L_t + CE
H 1021-1	4	BF	5.0	5.3	5.7	1.7	2.7	31.7	2.0	10.0	22.7	5.3	8.0	16.0	36.3	47.3	38.0	74.3	8.0	85.3
H 1021-2	4	BF	15.3	12.0	7.0	3.0	16.3	1.0	0.3	9.3	15.7	13.0	7.0	34.3	17.7	36.7	38.0	55.7	28.3	74.7
H 1021-3	4	BF	14.3	8.7	8.0	2.7	18.3	0.7	1.7	10.0	25.3	4.7	5.7	31.0	20.7	37.3	40.0	60.7	27.0	77.3
H 1021-5	4	BF	19.2	13.2	5.5	4.0	13.8	0.5	1.6	9.9	20.1	6.2	6.1	37.9	15.9	34.6	36.2	52.1	27.0	70.8
H 1021-6	4	BF	21.3	5.7	5.0	0.3	13.3	0.7	0.0	16.7	24.7	7.7	4.7	32.0	14.0	24.7	49.0	63.0	19.0	73.7
H 1021-7	4	BF	1.0	5.7	9.7	0.7	8.3	18.0	0.3	16.7	25.7	6.0	8.0	16.3	26.7	42.0	48.3	75.0	14.0	90.3
H 1021-8	4	BF	0.3	7.3	22.3	0.0	2.7	20.3	0.7	10.0	23.7	2.0	10.7	30.0	23.7	53.3	35.7	59.3	10.0	89.0
H 1021-10	6	BF	7.0	7.0	6.0	2.0	6.0	13.5	0.0	14.5	32.0	8.5	3.5	20.0	19.5	32.5	55.0	74.5	13.0	87.5
H 1021-12	6	BF	4.0	2.0	10.3	0.3	1.7	7.3	0.3	6.7	38.7	20.7	8.0	16.3	9.3	21.7	66.0	75.3	3.7	87.7
H 1021-13	6	BF	3.7	2.7	5.3	0.3	0.7	9.7	0.0	8.0	34.3	31.3	4.0	11.7	10.3	18.3	73.7	84.0	3.3	92.0
H 1021-14	6	BF	6.0	5.5	9.5	0.0	7.0	7.0	0.0	2.5	22.5	34.0	6.0	21.0	14.0	29.0	59.0	73.0	12.5	88.0
EY 1-1	5	BF	7.3	8.3	6.7	2.3	10.3	26.0	0.7	7.3	21.3	5.7	4.0	22.3	37.0	52.0	34.3	71.3	18.7	86.3
EY 1-3	5	BF	4.3	4.0	7.7	1.0	5.3	7.3	0.0	20.3	36.7	7.7	5.7	16.0	12.7	24.3	64.7	77.3	9.3	89.0
EY 1-4	5	BF	9.3	5.7	6.3	2.7	8.3	11.7	0.3	9.3	30.3	9.7	6.3	21.3	20.3	32.3	49.3	69.7	14.0	81.7
EY 1-6	5	BF	6.3	8.7	6.7	1.7	8.7	15.0	0.7	9.7	31.7	7.7	3.3	21.7	24.3	39.7	49.0	73.4	17.3	88.7
EY 1-7	5	BF	7.0	6.0	8.7	1.0	7.3	16.7	0.7	11.7	28.7	9.3	3.0	21.7	24.7	39.3	49.7	74.3	13.3	89.0
EY 1-8	15	LF	8.5	11.5	9.5	1.5	7.5	2.5	0.0	1.0	54.0	2.0	2.0	29.5	10.0	31.0	57.0	67.0	19.0	88.0
EY 1-9	15	LF	13.0	9.8	3.8	0.3	3.5	5.8	0.3	16.5	39.0	5.5	2.8	26.5	9.5	23.0	61.0	70.5	13.3	84.0
EY 1-11	8	BF	6.3	5.0	5.7	1.7	14.3	2.0	0.3	1.7	41.7	17.3	4.0	17.0	16.7	27.3	60.7	77.3	19.3	88.0
EY 2-2	2	RF	16.3	3.7	11.0	3.7	8.0	11.3	0.7	15.3	20.0	0.0	10.0	31.0	20.0	34.7	35.3	55.3	11.7	70.0
EY 2-6	2	RF	3.0	0.0	31.5	0.5	6.5	4.5	0.0	19.5	31.5	2.0	1.0	34.5	11.0	42.5	53.0	64.0	6.5	95.5
EY 2-10	2	RF	9.0	3.7	4.3	1.3	7.7	10.3	0.3	20.3	35.0	0.7	7.3	17.0	18.3	26.3	56.0	74.3	11.3	82.3
EY 2-11	3	RF	1.0	0.0	39.0	0.5	7.5	6.5	0.0	6.0	33.5	1.0	5.0	40.0	14.0	53.0	40.5	54.5	7.5	93.5
EY 2-13	3	RF	6.3	3.3	5.3	2.7	8.3	17.7	2.0	10.7	32.0	5.0	6.7	15.0	28.0	36.7	47.7	75.7	11.7	84.3
EY 2-14	3	RF	3.3	6.0	7.3	1.3	6.3	19.0	3.3	10.3	40.0	1.3	1.7	16.7	28.7	42.0	51.7	80.3	12.3	93.7
EY 2-16	3	RF	8.5	5.0	8.5	3.0	9.0	14.0	1.0	13.5	32.5	1.0	4.0	22.0	24.0	37.5	47.0	71.0	14.0	84.5
EY 2-17	3	RF	10.5	4.0	3.0	1.5	5.5	10.5	0.5	17.0	42.0	2.0	3.5	17.5	16.5	23.5	61.0	77.5	9.5	84.5
EY 3-1	7	TLF	4.3	7.7	13.3	0.7	15.3	4.7	0.0	3.7	10.7	37.3	2.3	25.3	20.0	41.0	51.7	71.7	23.0	92.7
EY 3-4	7	BF	7.0	10.0	16.7	1.0	5.7	28.0	1.0	7.7	15.3	4.3	3.3	33.7	34.7	61.3	27.3	62.0	15.7	88.7
EY 3-8	7	TLF	15.7	13.7	6.7	2.7	22.0	0.3	1.0	4.7	23.3	3.0	7.0	36.0	23.3	43.7	31.0	54.3	35.7	74.7
EY 3-9	7	TLF	17.7	18.7	5.0	2.3	22.0	0.0	0.7	2.0	18.7	4.3	8.7	41.3	22.7	46.3	25.0	47.7	40.7	71.3
EY 3-11	7	BF	7.0	9.0	13.7	2.3	6.7	24.3	1.3	3.7	16.7	11.3	4.0	29.7	32.3	55.0	31.7	64.0	15.7	86.7
EY 3-12	7	BF	7.7	7.7	6.0	0.7	10.7	22.0	0.3	7.3	19.3	12.3	6.0	21.3	33.0	46.7	39.0	72.0	18.3	85.7
EY 3-13	7	BF	9.3	17.0	6.0	3.7	6.7	19.0	1.7	6.0	19.3	6.3	5.0	32.3	27.3	50.3	31.7	59.0	23.7	82.0
EY 3-14	1	TLF	20.7	11.3	7.3	2.7	14.7	1.3	1.7	8.0	22.3	3.3	6.7	39.3	17.7	36.3	33.7	51.3	26.0	70.0
EY 4-1	10	BF	6.0	9.7	4.0	1.7	9.3	0.3	0.3	10.7	37.3	17.0	3.7	19.7	10.0	23.7	65.0	75.0	19.0	88.7
EY 4-2	10	BF	5.3	10.0	6.0	1.3	8.3	1.7	0.0	17.0	25.7	18.0	6.7	21.3	10.0	26.0	60.7	70.7	18.3	86.7
EY 4-3	10	BF	5.1	3.6	5.2	0.9	4.3	0.3	0.4	33.2	32.2	8.6	6.1	13.9	5.0	13.8	74.0	79.0	7.9	87.8
EY 4-5	10	BF	3.7	5.3	7.3	0.7	4.3	0.0	0.0	33.7	29.7	10.3	5.0	16.3	4.3	17.0	73.7	78.0	9.7	90.7

Table 1 (continued)

Sample No.	Loc. No.	Sed. Succ.	Light mineral data																
			Q_m	Q_p	Q_c	F	L_{sm}	L_u	L_v	C_m	C_s	D	Others	Q	L	L_t	CE	L + CE	M	L_t + CE
EY 5-4	11	LF	5.0	6.0	11.7	2.0	6.3	0.0	0.7	2.7	55.3	9.0	1.3	22.7	7.0	24.7	67.0	74.0	12.3	91.7
EY 5-9	11	LF	12.0	10.3	7.0	4.3	12.7	0.0	0.0	2.7	46.0	2.0	3.0	29.3	12.7	30.0	50.7	63.3	23.0	80.7
EY 5-10	11	LF	14.3	14.7	4.0	4.3	8.7	0.7	0.7	1.3	44.7	2.0	4.7	33.0	10.0	28.7	48.0	58.0	23.3	76.7
EY 5-16	13	LF	20.3	7.7	5.3	4.7	17.7	1.3	1.0	5.0	31.0	2.0	4.0	33.3	20.0	33.0	38.0	58.0	25.3	71.0
EY 5-18	13	LF	18.3	19.0	10.0	3.0	14.7	2.0	2.3	2.0	24.0	2.0	2.7	47.3	19.0	48.0	28.0	47.0	33.7	76.0
EY 5-19	13	LF	13.0	18.7	6.3	7.7	11.3	0.0	2.0	17.0	21.3	1.0	1.7	38.0	13.3	38.3	39.3	52.7	30.0	77.7
EY 5-21	13	LF	3.5	4.5	12.0	3.5	6.0	1.0	1.5	10.5	56.0	0.0	1.5	20.0	8.5	25.0	66.5	75.0	10.5	91.5
EY 5-22	13	LF	4.5	6.0	8.0	4.0	5.5	2.0	0.0	7.0	61.5	0.0	1.5	18.5	7.5	21.5	68.5	76.0	11.5	90.0
EY 6-1	7	TLF	15.3	6.3	6.0	2.7	9.7	0.0	0.7	16.7	28.3	6.3	8.0	27.7	10.3	22.7	51.3	81.7	16.0	74.0
EY 6-4	7	TLF	23.3	14.3	8.3	2.0	12.0	0.0	0.3	2.7	18.0	3.0	16.0	46.0	12.3	35.0	23.7	36.0	26.3	58.7
EY 6-5	7	TLF	19.7	18.7	4.7	3.3	11.3	1.3	0.3	7.7	19.3	2.0	11.7	43.0	13.0	36.3	29.0	42.0	30.0	65.3
EY 7-5	12	LF	12.0	12.7	8.3	4.0	12.0	2.3	0.7	12.3	27.0	6.0	2.7	33.0	15.0	36.0	45.3	60.3	24.7	81.3
EY 7-7	12	LF	2.7	12.0	1.7	1.0	9.3	0.7	2.0	14.0	47.3	0.3	9.0	16.3	12.0	25.7	61.7	73.7	21.3	87.3
EY 7-9	12	LF	13.3	18.0	6.0	4.3	11.0	1.7	0.3	10.0	27.0	4.0	4.3	37.3	13.0	37.0	41.0	54.0	29.0	78.0
EY 7-16A	12	LF	8.7	26.3	9.0	2.3	15.7	0.0	0.0	8.7	25.7	1.0	2.7	44.0	15.7	51.0	35.3	51.0	42.0	86.3
EY 7-16B	12	LF	4.3	24.0	5.3	1.0	13.3	0.3	1.0	5.0	40.3	3.0	2.4	33.7	14.7	44.0	48.3	63.0	37.3	92.3
EY 8-5	13	LF	24.7	11.3	8.0	5.0	9.0	1.0	2.0	5.0	29.3	1.0	3.7	44.0	12.0	31.3	35.3	47.3	20.3	66.7
EY 8-8	13	LF	13.7	10.0	2.3	5.0	8.7	1.3	1.0	21.0	32.3	3.7	1.0	26.0	11.0	23.3	57.0	68.0	18.7	80.3
EY 8-11	13	LF	18.0	13.7	3.3	6.3	7.7	1.7	0.3	2.3	39.7	2.3	4.7	35.0	9.7	26.7	44.3	54.0	21.3	71.0
EY 8-13	13	LF	13.3	29.3	10.3	2.7	17.7	2.3	5.0	0.0	17.0	0.3	2.0	53.0	25.0	64.7	17.3	42.3	47.0	82.0
EY 8-15	13	LF	9.7	23.0	8.0	5.3	16.3	5.0	6.0	0.3	19.3	2.0	5.0	40.7	27.3	58.3	21.7	49.0	39.3	80.0
EY 8-16	13	LF	13.0	13.5	11.0	6.0	14.5	2.5	3.0	0.5	27.5	2.0	6.5	37.5	20.0	44.5	30.0	50.0	28.0	74.5
EY 8-17	13	LF	10.0	12.5	5.0	3.5	12.5	0.0	1.0	24.5	26.5	2.0	2.5	27.5	13.5	31.0	53.0	66.5	25.0	84.0
EY 8-20	13	LF	18.3	19.7	5.7	3.7	12.0	1.0	1.3	5.3	30.3	0.3	2.3	43.7	14.3	39.7	36.0	50.3	31.7	75.7
EY 8-22	13	LF	8.0	11.5	2.0	1.0	2.5	0.5	0.0	21.0	47.5	3.0	3.0	21.5	3.0	16.5	71.5	74.5	14.0	88.0
EY 8-24A	13	LF	4.5	10.0	6.5	4.5	14.5	5.0	0.5	3.0	40.5	6.0	5.0	21.0	20.0	36.5	49.5	69.5	24.5	86.0
EY 8-24C	13	LF	3.7	4.7	6.7	2.0	4.3	1.7	1.0	13.7	44.7	2.7	15.0	15.0	7.0	18.3	61.0	68.0	9.0	79.4
EY 8-25	13	LF	11.0	12.7	7.7	4.3	20.3	1.3	2.7	3.7	28.7	3.3	4.3	31.3	24.3	44.7	35.7	60.0	33.0	80.3
EY 8-30	13	LF	13.0	9.7	3.0	1.0	3.7	0.0	0.3	20.0	46.7	0.3	2.3	25.7	4.0	16.7	67.0	71.0	13.3	83.7
EY 9-16	8	BF	4.0	3.7	3.3	0.3	8.3	0.7	0.0	37.7	34.7	3.0	4.3	11.0	9.0	16.0	75.3	84.3	12.0	91.3
EY 9-24	8	LF	17.7	36.7	7.0	3.3	13.3	0.0	0.3	1.0	17.3	2.7	0.7	61.3	13.7	57.3	21.0	34.7	50.0	78.3
EY 9-26C	8	BF	8.0	9.5	8.0	4.0	4.5	0.0	0.5	9.0	38.5	15.5	2.5	25.5	5.0	22.5	63.0	68.0	14.0	85.5
EY 9-30	8	BF	2.0	3.3	5.0	0.3	8.7	2.3	2.7	27.7	34.7	9.0	4.3	10.3	13.7	22.0	71.3	85.0	12.0	93.3
EY 9-31	8	BF	2.8	2.9	2.7	1.2	8.2	2.2	0.1	33.6	26.4	12.1	7.6	8.4	10.5	16.1	72.2	82.7	11.1	88.3
EY 9-34	8	BF	3.7	9.3	6.3	1.3	5.7	1.3	0.3	25.7	28.7	10.0	7.7	19.3	7.3	23.0	64.3	71.7	15.0	87.3
EY 9-36	8	BF	8.0	8.5	3.0	0.0	1.0	0.0	0.0	21.0	53.5	2.0	3.0	19.5	1.0	12.5	76.5	77.5	9.5	89.0
EY 9-37	8	BF	12.5	30.5	11.0	1.5	16.5	4.0	2.0	6.5	8.0	5.5	2.0	54.0	22.5	64.0	20.0	42.5	47.0	84.0
EY 12-1	17	?LF	6.0	2.5	9.5	5.0	14.5	1.5	0.5	9.0	44.5	1.0	6.0	18.0	16.5	28.5	54.5	71.0	17.0	83.0
EY 12-2	17	?LF	41.0	16.5	4.0	9.0	6.5	1.0	0.0	0.0	10.5	2.0	9.5	61.5	7.5	28.0	12.5	20.0	23.0	40.5
EY 12-8	14	LF	13.5	6.5	18.5	4.5	7.0	0.0	0.0	1.0	45.0	0.0	4.0	38.5	7.0	32.0	46.0	53.0	13.5	78.0
EY 12-17	16	LF	6.7	3.7	8.3	4.3	23.3	1.0	2.7	7.0	36.7	1.3	5.0	18.7	27.0	39.0	45.0	72.0	27.0	84.0

Table 1 (continued)

Sample No.	Loc. No.	Sed. Succ.	Light mineral data																
			Q_m	Q_p	Q_c	F	L_{sm}	L_u	L_v	C_m	C_s	D	Others	Q	L	L_t	CE	L + CE	M	L_t + CE
EY 13-13	15	LF	12.0	5.7	8.7	2.3	6.0	0.7	0.0	6.0	52.3	2.7	3.7	26.3	6.7	21.0	61.0	67.7	11.7	82.0
EY 13-19	15	LF	15.7	9.0	9.0	2.7	8.3	1.3	0.0	7.0	41.3	2.3	3.3	33.7	9.7	27.7	50.7	60.3	17.3	78.3
EY 13-21	15	LF	3.3	0.0	12.7	3.3	0.7	0.0	0.0	6.3	60.0	4.3	9.3	16.0	0.7	13.3	70.7	71.3	0.7	84.0
EY 16-2	9	BF	16.5	0.0	11.5	1.5	0.0	0.0	0.0	0.5	0.5	47.5	22.0	28.0	0.0	11.5	48.5	48.5	0.0	60.0
EY 16-6	8	BF	10.8	2.5	8.5	1.8	5.8	2.0	1.0	19.8	33.5	8.3	6.3	21.8	8.8	19.8	61.5	70.3	8.3	81.3
EY 16-7	8	BF	9.0	5.0	15.7	1.3	8.3	0.3	1.3	6.0	31.0	14.7	7.3	29.7	10.0	30.7	51.7	61.7	13.3	82.3
EY 16-8	8	BF	7.3	10.3	11.0	0.7	8.3	0.3	3.7	4.7	19.0	31.3	3.3	28.7	12.3	33.7	55.0	67.3	18.7	88.7
EY 16-13	8	BF	3.7	4.0	4.7	1.0	12.3	4.0	0.0	30.3	21.7	12.0	6.3	12.3	16.3	25.0	64.0	80.3	16.3	89.0

Sample No.	Loc. No.	Sed. Succ.	Heavy mineral data												Mineral chemistry
			chr	zrn	tur	rt	grt	cld	gln	epi	am/g	ap	others	ZTR	META	
H 1021-1	4	BF	81.5	2.0	1.5	0.0	5.0	0.5	0.5	0.5	1.5	0.5	6.5	3.5	8.0	mi
H 1021-2	4	BF	33.5	9.0	22.0	6.0	0.5	13.5	3.5	3.0	0.0	8.0	1.0	37.0	20.5	
H 1021-5	4	BF	20.4	7.9	33.8	4.8	1.9	15.0	6.8	1.4	0.1	6.6	1.4	46.5	25.1	mi, tur, grt, cld, gln
H 1021-6	4	BF	17.0	11.0	27.0	4.0	1.0	7.5	18.5	4.0	1.0	8.0	1.0	42.0	32.0	
H 1021-7	4	BF	85.0	1.5	2.5	0.0	3.0	1.5	1.0	2.0	2.0	0.0	1.5	4.0	9.5	
H 1021-10	6	BF	25.4	16.9	15.3	10.1	11.9	5.1	10.2	1.7	0.0	0.0	3.4	42.3	28.9	
H 1021-12	6	BF	79.0	2.0	6.0	1.0	5.0	3.5	1.5	0.5	0.5	1.0	0.0	9.0	11.0	
H 1021-13	6	BF	85.5	1.5	5.0	2.5	1.0	1.0	1.5	0.5	0.0	1.0	0.5	9.0	4.0	
EY 1-1	5	BF	89.5	2.0	2.5	0.5	1.0	0.0	1.5	0.0	0.0	3.0	0.0	5.0	2.5	
EY 1-3	5	BF	75.5	6.0	3.5	3.5	3.0	1.0	3.0	3.0	0.0	1.5	0.0	13.0	10.0	mi, gln
EY 1-4	5	BF	77.0	4.0	3.5	1.0	2.0	2.0	4.0	3.5	0.0	2.0	1.0	8.5	11.5	
EY 1-6	5	BF	86.5	2.5	3.0	0.5	0.5	1.5	1.5	2.0	1.5	0.5	0.0	6.0	7.0	
EY 1-9	15	LF	87.5	4.5	5.0	0.5	0.0	0.0	0.0	1.5	0.0	1.0	0.0	10.0	1.5	mi
EY 1-11	8	BF	84.5	2.0	9.5	1.5	0.5	0.5	0.0	0.0	0.0	1.5	0.0	13.0	1.0	
EY 2-2	2	RF	23.0	2.5	1.0	0.5	2.0	0.0	0.5	1.5	64.0	1.5	3.5	4.0	68.0	gln, am/g
EY 2-6	2	RF	90.0	3.0	1.0	0.0	1.0	0.0	0.0	2.5	2.0	0.0	0.5	4.0	5.5	mi
EY 2-10	2	RF	16.0	1.5	1.0	0.0	0.0	0.0	0.0	0.5	78.0	0.0	3.0	2.5	78.5	am/g
EY 2-11	3	RF	86.5	5.0	6.0	0.5	0.5	0.0	0.5	0.0	1.0	0.0	0.0	11.5	2.0	
EY 2-14	3	RF	94.0	0.5	0.5	0.5	3.0	0.0	0.0	0.5	0.5	0.5	0.0	1.5	4.0	mi, grt
EY 2-16	3	RF	87.0	3.5	2.0	0.5	4.0	0.0	0.5	1.0	0.5	1.0	0.0	6.0	6.0	
EY 3-4	7	BF	90.5	2.5	0.5	0.5	2.5	0.0	0.5	0.0	2.0	0.5	0.5	3.5	5.0	
EY 3-8	7	TLF	6.5	12.5	12.8	5.3	19.8	31.8	0.8	2.8	0.3	5.8	2.0	30.6	55.3	
EY 3-9	7	TLF	8.2	12.2	8.4	4.6	17.4	35.9	0.7	2.2	0.1	7.2	3.1	25.2	56.3	mi, grt, cld
EY 3-11	7	BF	92.5	4.5	1.0	0.0	0.5	0.5	0.5	0.0	0.0	0.0	0.5	5.5	1.5	
EY 3-13	7	BF	96.0	2.0	1.0	0.5	0.0	0.0	0.5	0.0	0.0	0.0	0.0	3.5	0.5	
EY 3-14	1	TLF	13.6	24.5	28.3	9.7	3.8	4.7	3.0	0.6	0.1	9.4	2.3	62.5	12.2	mi, grt, gln
EY 4-1	10	BF	57.0	9.0	16.0	2.5	3.0	2.5	0.0	4.0	1.0	3.5	1.5	27.5	10.5	
EY 4-2	10	BF	72.5	2.5	9.0	2.0	5.0	3.0	0.0	1.5	0.5	2.0	2.0	13.5	10.0	

Table 1 (continued)

Sample No.	Loc. No.	Sed. Succ.	Heavy mineral data												Mineral chemistry
			chr	zrn	tur	rt	grt	cld	gln	epi	am/g	ap	others	ZTR	META	
EY 4-3	10	BF	73.0	1.5	5.0	1.0	8.0	4.0	2.5	0.0	0.0	3.5	1.5	7.5	14.5	mi, grt, gln
EY 4-5	10	BF	65.5	2.0	9.0	0.3	4.0	4.0	3.5	0.3	0.0	2.5	9.0	11.3	11.8	
EY 5-4	11	LF	43.0	17.0	16.5	9.0	0.0	0.0	0.0	1.0	0.0	7.0	6.5	42.5	1.0	
EY 5-10	11	LF	5.3	2.7	18.0	8.7	0.0	0.0	0.7	0.0	0.0	0.0	64.7	29.4	0.7	mi
EY 5-16	13	LF	76.0	11.0	4.0	4.0	2.0	0.0	0.0	0.0	0.0	2.0	1.0	19.0	2.0	
EY 6-1	7	TLF	18.0	8.0	36.0	5.5	1.0	17.0	0.5	0.5	0.0	12.5	1.0	49.5	19.0	tur, cld
EY 6-4	7	TLF	8.5	10.5	42.5	8.5	0.5	5.5	0.0	0.0	0.5	22.5	1.0	61.5	6.5	
EY 6-5	7	TLF	9.5	15.0	33.0	12.5	0.0	6.5	0.0	0.0	0.0	23.0	0.5	60.5	6.5	mi
EY 7-5	12	LF	75.5	10.5	5.5	1.5	1.5	0.5	0.0	0.0	0.0	4.0	1.0	17.5	2.0	mi
EY 7-9	12	LF	86.0	5.5	0.0	2.5	0.5	0.0	0.0	0.5	0.0	2.5	2.5	8.0	1.0	
EY 7-16B	12	LF	70.5	9.0	2.5	1.0	4.5	0.0	0.0	0.0	0.0	6.5	6.0	12.5	4.5	grt
EY 8-5	13	LF	86.5	6.5	2.5	0.0	0.0	0.0	0.0	0.0	0.0	4.0	0.5	9.0	0.0	
EY 8-8	13	LF	72.5	6.0	11.5	1.5	0.0	0.0	0.0	0.5	0.0	7.0	1.0	19.0	0.5	
EY 8-15	13	LF	87.5	4.0	0.5	3.0	0.5	0.0	0.0	0.0	0.0	2.0	2.5	7.5	0.5	mi
EY 8-25	13	LF	59.7	8.3	6.3	2.0	0.0	0.0	0.0	0.3	0.0	6.0	17.3	16.6	0.3	
EY 9-16	8	BF	74.5	10.0	3.0	2.0	0.0	2.5	0.0	1.5	0.0	6.5	0.0	15.0	4.0	mi
EY 9-30	8	BF	71.0	3.0	2.5	0.5	6.0	2.0	0.0	0.5	0.0	8.5	6.0	6.0	8.5	mi
EY 9-31	8	BF	61.0	4.0	3.0	1.0	24.0	1.0	0.0	1.0	0.0	2.0	3.0	8.0	26.0	
EY 9-34	8	BF	77.3	3.8	4.5	1.5	5.0	2.8	0.8	0.5	0.0	0.5	2.2	9.8	10.2	mi, tur, grt, cld, gln
EY 13-19	15	LF	83.5	3.5	6.5	0.5	0.0	0.0	0.0	0.0	0.0	1.5	4.5	10.5	0.0	
EY 13-21	15	LF	87.0	1.0	4.5	2.0	0.0	0.0	0.0	0.0	0.0	1.5	4.0	7.5	0.0	
EY 16-6	8	BF	62.0	5.5	11.0	3.0	5.5	10.0	1.0	0.5	0.0	0.0	1.5	19.5	17.0	
EY 16-7	8	BF	46.0	8.0	24.0	3.0	2.0	9.0	0.0	0.0	0.0	3.0	5.0	35.0	11.0	
EY 16-8	8	BF	14.0	31.0	31.0	15.0	0.0	1.5	0.0	1.0	0.0	2.0	4.5	77.0	2.5	
EY 16-13	8	BF														mi, grt (clasts)

For locality numbers see Fig. 4. For sedimentary successions see Fig. 3.

Q_c = chert; L_u = ultrabasic lithoclast (serpentinite); C_m = micritic calcite clast; C_s = sparitic calcite clast; D = dolomite clast; Others = mica + chlorite + glauconite + heavy minerals + intraclasts + bioclasts; Q = total quartzose grains ($Q_m + Q_p + Q_c$); L_t = total non-carbonate lithoclasts ($Q_p + Q_c + L_{sm} + L_u + L_v$); CE = carbonate extrabasinal clasts ($C_m + C_s$ + D); M = metamorphic clasts ($L_{sm} + Q_p$); chr = chrome spinel; zrn = zircon; tur = tourmaline; rt = rutile grt = garnet; cld = chloritoid; gln = blue sodic amphibole; epi = epidote group minerals; am/g = green calcic amphibole; ap = apatite; others = brookite/anatase + baryte + brown calcic amphibole + tremolite + anhydrite; ZTR = zrn + tur + rt; META = grt + cld + gln + epi + am/g; mi = white mica.

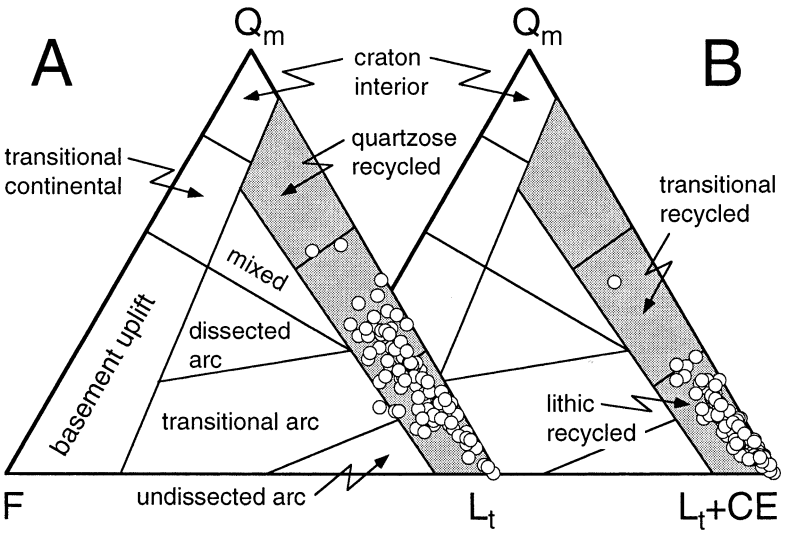

Fig. 6. Representation of the light mineral data set within the Q_mFL_t provenance diagram of Dickinson (1985): (A) lithoclasts including polycrystalline quartz grains but precluding carbonate clasts, (B) total lithoclasts including the carbonate extrabasinal clasts (*CE*). Both diagrams suggest a recycled orogen provenance of the litharenites.

(1) Metamorphic lithoclasts (M); this class comprises both Q_p and L_{sm} grains because they correlate positively with each other ($r = 0.98$, $n = 88$; von Eynatten, 1996) indicating that both grain types are derived from metamorphic source rocks, most probably of continental crustal origin.

(2) Serpentinite clasts (L_u); they indicate erosion of an ultrabasic source rock, most probably of oceanic crustal origin.

(3) Dolomite clasts (D); they give a more specific information than calcitic CE-clasts because they are largely restricted to the Upper Triassic Hauptdolomite Formation, whereas calcitic CE-clasts (C_m and C_s) may originate from the whole Mesozoic stratigraphic column of the NCA.

(4) Monocrystalline quartz grains (Q_m); they indicate either metamorphic source rocks or, depending on additional information, recycling of older (meta)sedimentary rocks. Furthermore, Q_m is a measure for the maturity of the sediment.

These four classes of light mineral grains are used to establish the diagram $\ln(L_u/M)$ vs. $\ln(D/Q_m)$ (Fig. 8). Logratio transformations are most suitable for the statistical analysis of compositional data sets

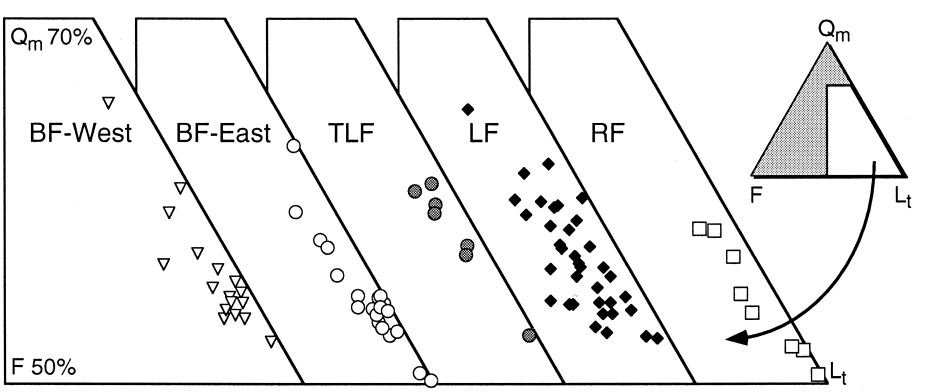

Fig. 7. Representation of the light mineral data of the individual sedimentary successions within the Q_mFL_t diagram (precluding CE-clasts). BF samples are subdivided into a western (*BF-West*) and a eastern group (*BF-East*).

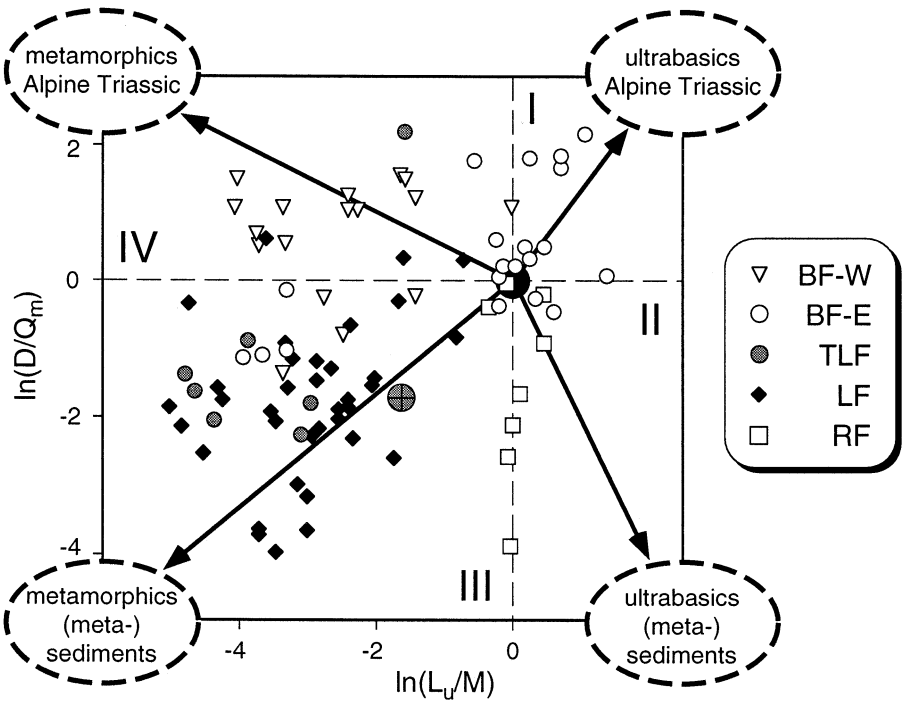

Fig. 8. Representation of the light mineral data within the logratio diagram $\ln(L_u/M)$ vs. $\ln(D/Q_m)$. The big grey circle with black cross inside indicates the average of nine TLF samples from Gaupp (1982). For further explanation see text.

(Aitchison, 1982; for review see Weltje, 1994). This diagram facilitates the use of four components and allows a reasonable discrimination between the four sedimentary successions and a quick determination of possible major source rocks for each succession (Fig. 8). The latter is done by subdividing the diagram into four quadrants with $\ln = 0$ (equivalent to a ratio of 1 : 1) as limiting value on both axes. Hence, two source rock lithologies are assigned to each quadrant (e.g., ultrabasic rocks and Alpine Triassic carbonates in case of quadrant I) based on which component is predominant in each of the two ratios (e.g., $L_u > M$ and $D > Q_m$ in case of quadrant I). All of the major light mineral grain types are included in the diagram except for calcitic CE-clasts (C_m and C_s). Because the contribution of $C_m + C_s$ to the framework grain spectrum usually ranges between 20% and 60%, a significant amount of calcitic carbonate source rocks has to be considered for all of the sedimentary successions.

The sandstones of the RF plot into quadrants II and III indicating the occurrence of Permo–Carboniferous (meta)sediments and metamorphic as well as ultrabasic rocks in the source area (Fig. 8). Samples from LF and TLF generally plot in quadrant III, the only difference being that LF sandstones display a wider range in D/Q_m ratios. Data from both formations suggest that metamorphic and (meta)sedimentary rocks are predominant in the source area. Based on light mineral data alone LF and TLF cannot be distinguished. Sandstones of the BF are characterized by higher D/Q_m ratios compared to all of the other sample groups. This implies a dominance of dolomitic over (meta)sedimentary source rocks and/or a less mature sediment where carbonate clasts are not diminished by chemical/physical abrasion. L_u/M ratios of BF samples seem to depend on sample location. In samples from the eastern part of the study area (e.g., BF type-locality) ultrabasic source rocks are more important than metamorphic source rocks, but towards the west the influence of ultrabasic source rocks is significantly lower. This is most likely a primary effect because otherwise the decreasing L_u/M ratios

should positively correlate with increasing sediment maturity (decreasing D/Q_m ratios), which is not the case.

This first approximation of provenance that is solely based on light mineral data will be tested in Sections 6 and 7 using heavy mineral data, and in Section 8 using mineral chemistry data.

5.3. Climate and relief

The influence of climate and relief on sandstone framework composition has long been known but its exact quantification remains a problem even in modern sedimentary systems (e.g., Ibbeken and Schleyer, 1991). Grantham and Velbel (1988) defined a simple weathering index $wi = c \times r$, where c is the rate of weathering ('climate') and r is the residence time of the sediment in the weathering environment ('relief'). In ancient sedimentary systems the variables c and r cannot be determined accurately. Weltje (1994) introduced a semiquantitative approach which is based on modern fluvial sands with known source rock lithologies and different climatic and physiographic conditions. A semiquantitative weathering index is calculated from the above formula using estimates for c and r (Fig. 9A). The compositional data of the modern sands were plotted in the logratio diagram $\ln(Q/F)$ vs. $\ln(Q/L)$ and each sample group was combined with its specific weathering index. The resulting compositional trend defines a clear relationship between sandstone composition, weathering index, and source rock lithology (Fig. 9B).

The compositional framework grain data of the analyzed sandstones are plotted into the diagram $\ln(Q/F)$ vs. $\ln(Q/L + CE)$ (Fig. 9B). The carbonate clasts (CE) have to be included into total lithoclasts because they are especially sensitive indicators for both mechanical and chemical abrasion (Pettijohn et al., 1987, p. 46). More than 90% of the samples plot into the upper field of $wi = 0$ indicating a detrital spectrum with very low degrees of weathering and a mainly metamorphic parentage. Because the diagram is solely based on data from modern sediments, postsedimentary processes have to be considered. Diagenetic modifications are generally expected to reduce feldspar and lithoclast concentrations. This would shift the composition to higher Q contents and, consequently, higher apparent weathering indices. Therefore the observed low weathering indices cannot be explained by postsedimentary processes.

The Cretaceous climate was generally warm. Particularly, Albian to Campanian average temperatures were highest in the entire Phanerozoic. The relatively high eustatic sea level argues for large shallow-marine shelf areas. In combination with the

A

semi-quantitative weathering index (wi = c * r) (Weltje, 1994)		RELIEF (r) high, mountains 0	moderate, hills 1	low, plains 2
CLIMATE (c) (semi-)arid, mediterran.	0	0	0	0
temperate, subhumid	1	0	1	2
tropical, humid	2	0	2	4

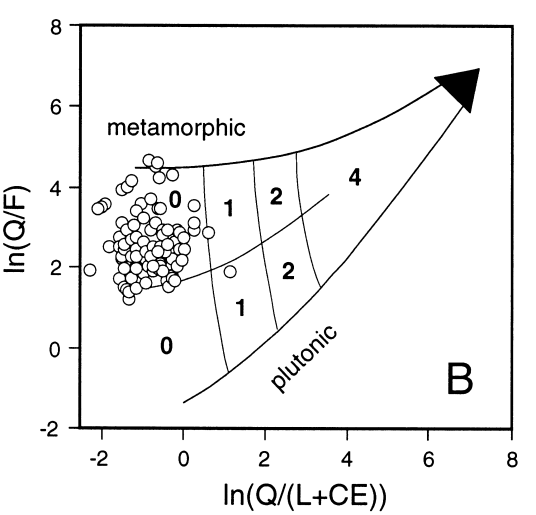

Fig. 9. (A) Semi-quantitative weathering index based on semi-quantitative estimates for climate and relief. (B) The analyzed samples indicate a very low weathering index ($wi = 0$) based on the light mineral data: $\ln(Q/(L + CE))$ vs. $\ln(Q/F)$. For further explanation see text and Weltje (1994).

elevated temperatures, evaporation and precipitation rates were presumably high. A (sub)tropical–(sub)humid climate can be assumed for the coastal areas of the Cretaceous Tethys (Flügel and Flügel-Kahler, 1992; Francis and Frakes, 1993). Fig. 9A suggests that very low weathering indices (wi = 0) combined with a (sub)tropical–(sub)humid climate ($c = 1$ to 2) call for a high-gradient, mountainous source area ($r = 0$). This is coincident with sedimentological models based on facies analysis of the studied sediments (e.g., Faupl and Tollmann, 1979; Gaupp, 1982; see Section 3).

Thus we conclude that the framework composition of the analyzed sandstones should closely resemble the potential spectrum of detritus defined by the source rocks. Some modifications cannot be excluded, but their extent is considered to be limited and restricted predominantly to physical abrasion. This situation is comparable to the recent situation in Calabria (Italy) where a high-gradient source area and high annual precipitation rates lead to a low residence time of the detrital material and, consequently, a very low degree of chemical weathering (Ibbeken and Schleyer, 1991).

6. Heavy mineral analysis

The heavy mineral spectra ($n = 52$) of the analyzed sedimentary rocks are mostly dominated by chrome spinel (chr, max. 96%, see Table 1 and Fig. 10). Chrome spinel is a common accessory phase in ultrabasic rocks and is generally thought to indicate an oceanic crustal provenance (Zimmerle, 1984). The chemistry of detrital chrome spinel in Cretaceous sandstones of the Eastern Alps supports this interpretation (Pober and Faupl, 1988). A second major group are the stable heavy minerals zircon, tourmaline, and rutile (ZTR, max. 77%). Minerals of this group are common in acidic to intermediate granitoid rocks as well as in mature siliciclastic sediments and some metamorphic rocks. They are generally thought to indicate a continental crustal provenance. Tourmaline usually displays the highest concentration of the ZTR-minerals (tourmaline > zircon > rutile). Further important heavy minerals are chloritoid (cld, max. 35.9%), garnet group minerals (grt, max. 24.0%), apatite (ap, max. 23.0%), and blue sodic amphibole (gln, max. 18.5%). Two samples show high concentrations of green calcic am-

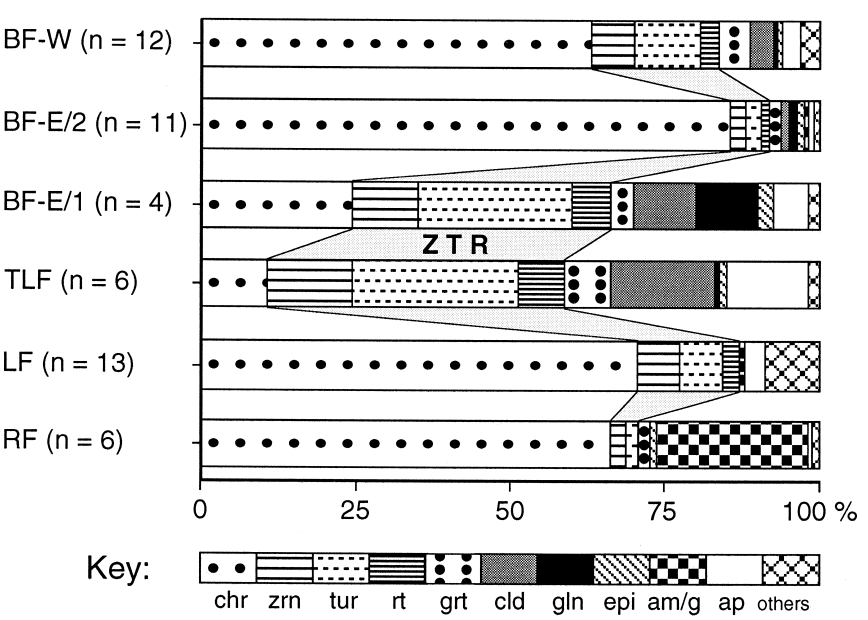

Fig. 10. Average heavy mineral spectra for the analyzed sedimentary successions (for individual samples see Table 1; *chr* = chrome spinel, *zrn* = zircon, *tur* = tourmaline, *rt* = rutile, *grt* = garnet, *cld* = chloritoid, *gln* = blue sodic amphibole, *epi* = epidote group minerals, *am/g* = green calcic amphibole, *ap* = apatite, *ZTR* = zrn + tur + rt). BF samples are divided into three subgroups due to contrasting heavy and light mineral compositions.

phibole up to 78.0%. Minor constituents are epidote group minerals (epi, max. 4.0%), brookite/anatase, anhydrite, tremolite, brown calcic amphibole, and baryte.

The heavy mineral spectra of sandstones of the RF are characterized by two endmember compositions. The first is dominated by chrome spinel (max. 94.0%) and the second is dominated by green calcic amphibole (max. 78%). Mixing between these endmember compositions is common (Faupl and Tollmann, 1979). Minor components are tourmaline, zircon, garnet, epidote, and brown calcic amphibole.

The major heavy mineral phase in samples from the LF is chrome spinel (max. 87.5%), whereas ZTR range from 7.5% to 29.4% (see also Winkler, 1988). Further species are apatite (max. 7.0%) and garnet (max. 4.5%). Two heavy mineral spectra show an exceptionally high baryte content (16.7% and 64.0%). Apart from two samples with concentrations of 0.7%, the heavy mineral spectra of the LF do not contain green calcic amphibole, chloritoid, and/or blue sodic amphibole.

Samples of the TLF show the highest concentrations of the stable heavy minerals ZTR (25.2%–62.5%) of all sample groups (Fig. 10). Chrome spinel is relatively low (6.5%–18.0%) but chloritoid, apatite, and garnet range up to 35.9%, 23.0%, and 19.8%, respectively. Minor components are blue sodic amphibole (max. 3.0%) and epidote group minerals (max. 2.8%).

The sandstones of the BF are subdivided into three sample groups. A suite of four samples (BF-E/1) is comparable to the TLF samples in terms of relatively low chrome spinel and high ZTR concentrations but differs due to lower concentrations of chloritoid and garnet and higher concentrations of blue sodic amphibole (max. 18.5%). A second group (BF-E/2) is characterized by the highest chrome spinel concentration (75.5–96.0%) of all sample groups and, consequently, ZTR-minerals are rare (3.5–13.0%). All samples contain blue sodic amphibole as a minor component (0.5–4.0%) and most of them additionally garnet (max. 5.0%), chloritoid (max. 3.5%) and epidote (max. 3.5%). The third group (BF-W) are samples from the westernmost occurrences of the BF and was already separated from the eastern sample groups (BF-E) based on light mineral data (Section 5.2). These samples are somewhat lower in chrome spinel (46.0–84.5%) and higher in ZTR concentration (6.0–35.0%) compared to BF-E/2. Garnet is slightly higher on average (max. 24.0%). All samples contain chloritoid (0.5–10.0%) and several samples contain epidote group minerals (max. 4.0%) and blue sodic amphibole (max. 3.5%). One sample of the BF-W group (EY 16-8) is exceptionally low in chrome spinel (14.0%) but has a very high ZTR-mineral content (77.0%).

Based on the heavy mineral data we assign the analyzed Cretaceous sedimentary rocks of the NCA to two major source areas: RF and LF to a southeastern source area, and TLF and BF to a northwestern source area. This interpretation is based on: (1) a widely accepted model which suggests that the sediments of the RF were shed from a source area southeast of the Austroalpine which includes the Meliata/Vardar suture zone (e.g., Decker et al., 1987; see Section 3); (2) a widely accepted model which suggests that the siliciclastic sediments of the TLF were shed from a source area northwest of the Upper Austroalpine most probably in a Lower Austroalpine to South Penninic position (e.g., Faupl and Wagreich, 1992; see Section 3); and (3) the exclusive occurrence of blue sodic amphibole and chloritoid in sedimentary rocks of the TLF and BF. The latter strongly argues for a derivation of the sediments of the BF from the same source area as the TLF (the northwestern source), because especially blue sodic amphibole is not a common heavy mineral phase. It is restricted to specific source rocks in specific tectonic settings (depending on composition, see Section 8.1.1) and is relatively unstable with respect to both physical and chemical abrasion (Morton, 1985). Consequently, blue sodic amphibole and chloritoid are the two characteristic heavy mineral phases for the northwestern source area.

These two minerals generally do not occur in sedimentary rocks of the LF and RF except for one grain of chloritoid in one sample of the LF and a few grains of blue sodic amphibole in one sample of the LF (0.7%) and in three samples of the RF (each 0.5%). The latter are different in composition compared to BF and TLF minerals (Section 8.1.1). The general lack of blue sodic amphibole and chloritoid in the sedimentary rocks of the LF may be explained in two ways: (1) these sediments were not derived from the northwestern source, or (2) blue

sodic amphibole and chloritoid are removed by intrastratal solution. The latter possibility has to be considered because the rocks of the LF were affected by a stronger postsedimentary overprint compared to those of TLF/BF (see Section 2) and amphibole especially is sensitive to intrastratal solution. However, chloritoid is more stable than amphibole and its resistance to intrastratal solution is comparable to that of garnet (Morton, 1985; Mange and Maurer, 1991). Garnet is found in five out of thirteen LF samples (max. 4.5%) and these grains give no evidence for extensive surface corrosion. We conclude that the absence of chloritoid in the heavy mineral spectra of the LF is not due to intrastratal solution, but is a primary feature of the source area of the LF. Consequently, the sedimentary rocks of the LF cannot have been derived from the northwestern source area. The second possible source of abundant chrome spinel in LF samples is the Meliata/Vardar suture zone to the southeast, from where the sediments of the RF originate. The lack of calcic amphibole in the LF compared to the RF can be explained by variations through time because there is no stratigraphic overlap between these two sedimentary successions (Fig. 3).

7. Heavy minerals vs. light minerals

Logratio diagrams relate light mineral spectra and heavy mineral spectra to each other by combining ratios of both data sets in a single x, y diagram. This may be useful for (1) attributing specific heavy mineral phases to specific lithoclast types, and (2) discriminating between sample groups based on two different data sets.

Fig. 11 shows the heavy mineral logratios $\ln(\mathrm{chr/ZTR})$, $\ln(\mathrm{chr/gln})$, and $\ln(\mathrm{chr/cld})$ in relation to the light mineral logratio $\ln(\mathrm{L_u/M})$. This light mineral ratio correlates positively ($r = 0.70$, $n = 52$, 99% confidence level) with the logratio between chrome spinel and ZTR (Fig. 11A). We conclude that chrome spinel is derived from the same source as the serpentinite fragments ($\mathrm{L_u}$). This is not trivial, because chrome spinel might be recycled from older sedimentary rocks. If the samples of the LF are considered separately the observed positive correlation between serpentinite and chrome spinel is not significant (high chr concentration but relative low $\mathrm{L_u}$ content). This may be explained by the higher maturity of LF sandstones (as suggested by low $\mathrm{D/Q_m}$ ratios, see Fig. 8) which causes a decrease of the mechanically unstable serpentinite fragments. The positive correlation of $\ln(\mathrm{L_u/M})$ and

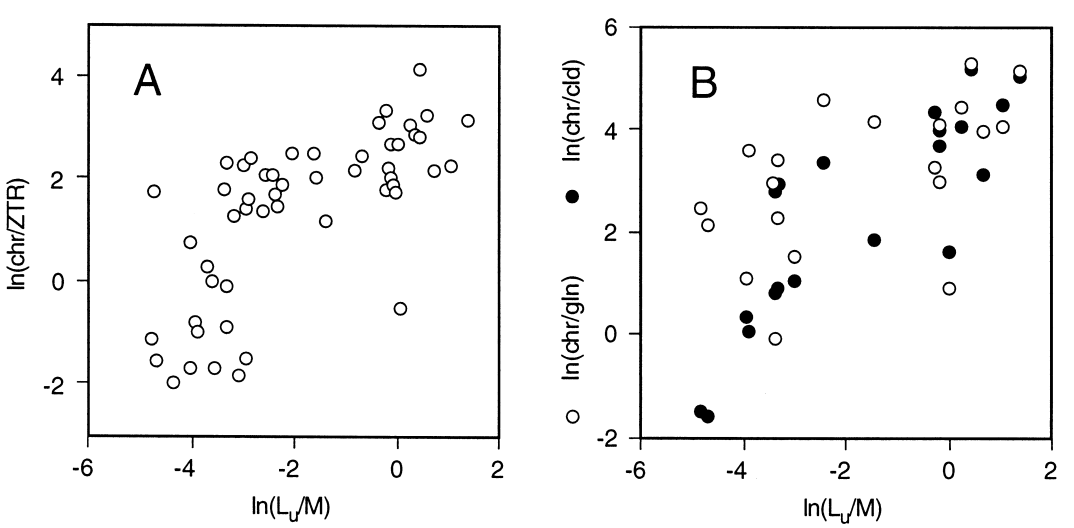

Fig. 11. Logratio diagrams with the light mineral parameter $\ln(\mathrm{L_u/M})$ on the x-axis and varying heavy mineral logratios on the y-axis: (A) $\ln(\mathrm{chr/ZTR})$ correlates positively with increasing $\mathrm{L_u/M}$ ratios ($r = 0.70$, $n = 52$); (B) $\ln(\mathrm{chr/gln})$ and $\ln(\mathrm{chr/cld})$ correlate positively with increasing $\mathrm{L_u/M}$ ratios at the 95% confidence level ($r = 0.55$) and 99% confidence level ($r = 0.85$), respectively (all samples of BF and TLF which contain both gln and cld, $n = 20$).

ln(chr/ZTR) further suggests that the stable heavy minerals ZTR are derived from the same source rocks as the metamorphic lithoclasts ($M = Q_p + L_{sm}$, see Section 5.2). The logratios between chrome spinel and both blue sodic amphibole and chloritoid correlate positively with increasing L_u/M ratios at 95% ($r = 0.55$, $n = 20$) and 99% confidence levels ($r = 0.85$, $n = 20$), respectively (Fig. 11B). We conclude that blue sodic amphibole and chloritoid are associated with quartzose metamorphic source rocks (Q_p, L_{sm}) and the stable heavy minerals ZTR and not with the ultrabasic source rock assemblage represented by L_u and chrome spinel (see also von Eynatten et al., 1997b).

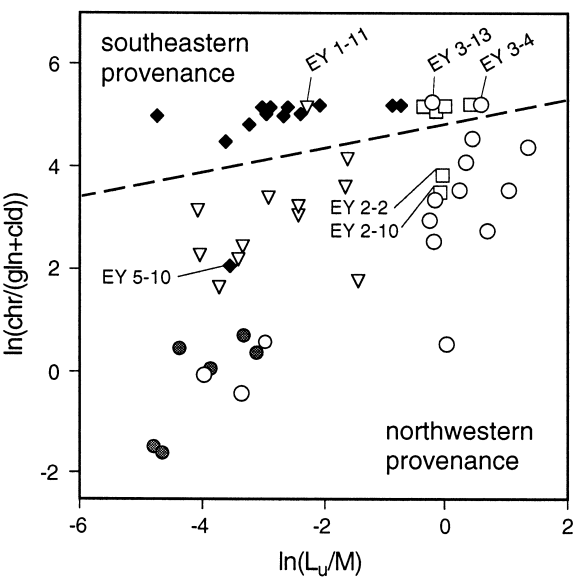

Fig. 12. Logratio diagram ln(L_u/M) vs. ln(chr/(gln + cld)) to discriminate between the sedimentary successions as well as the two provenance domains. For key see Fig. 8. Sample numbers indicate those samples that are exceptions (6 out of 52) from the suggested discrimination between northern and southern provenance. If gln + cld is zero, this value was replaced by 0.5, the smallest possible value according to 200 grain counts (Aitchison, 1982; von Eynatten, 1996). This is necessary due to simple mathematics but is responsible for the overlap of three BF samples with gln + cld as low as 0.5 (EY 1-11, EY 3-4, EY 3-13) with the southern provenance. Three more exceptions from the discrimination are given by RF samples EY 2-2 and EY 2-10 (two samples with low chr concentration due to very high contents of green calcic amphibole) and LF sample EY 5-10 (very low chr concentration due to extraordinary high baryte content, see Table 1).

The discrimination of the sedimentary successions based on light mineral data was only partly successful because of a strong overlap between LF and TLF sandstones and a partial overlap between LF and BF-W as well as RF and BF-E (Fig. 8). A logratio diagram of both light and heavy mineral data (e.g., ln(L_u/M) vs. ln(chr/(gln + cld)), Fig. 12) allows a better discrimination of the sandstones. This discrimination is based on the absence of blue sodic amphibole and chloritoid in sediments of southern provenance and the large range of L_u/M ratios. Despite six exceptions (out of 52 samples, Fig. 12) the discrimination between both the sedimentary successions and the two provenance areas is satisfying. The overlap between TLF and BF-E is explained by a continuous evolution in the northwestern source area and underlines the correlation of high gln + cld contents with low concentrations of chr and L_u.

8. Mineral chemistry

Microprobe analysis of detrital mineral phases serves as a tool to (1) verify optical mineral determinations, (2) identify mineral species and mineral aggregates unidentifiable by optical means, and (3) provide information on the chemical variation of specific mineral phases (Morton, 1991). The latter point is most stimulating because the chemical variability of mineral phases can be used to (1) discriminate between different source rocks, and (2) to obtain more specific information on the petrology of the source rock. The microprobe data are documented in detail in von Eynatten (1996). Data tables are available on request.

8.1. Amphibole

Amphiboles of various chemical composition are common minerals in several magmatic and metamorphic rocks and, consequently, occur in detrital sediments which are derived from these rock types. In contrast to the stable heavy minerals ZTR amphiboles are relatively unstable with respect to both chemical and mechanical abrasion. Therefore, mature sediments and/or sediments affected by diagenetic intrastratal solution may have totally lost these minerals. Amphiboles are often classified due to colour and other optical properties, but an un-

ambiguous nomenclature and, moreover, a genetic interpretation have to rely on chemical data (Leake, 1978; Mange and Maurer, 1991; Morton, 1991).

8.1.1. Blue sodic amphibole

Several studies have already demonstrated the importance of detrital glaucophane for the reconstruction of high-pressure (HP) metamorphic source rocks and, hence, the geodynamic evolution of mountain belts (e.g., Mange-Rajetzky, 1981; Misík and Sykora, 1981; Mange-Rajetzky and Oberhänsli, 1982; Winkler and Bernoulli, 1986; Till, 1992; Ganssloser et al., 1996). However, optical determination alone is not sufficient, because blue sodic amphiboles have a range of composition, e.g., from glaucophane to riebeckite. These two minerals cannot be unambiguously distinguished by optical means, but they do have different implications for source area geology: glaucophane, Fe-glaucophane and crossite originate from HP blueschist facies rocks, whereas riebeckite, Mg-riebeckite, and high-Fe^{3+} crossite come from either acid magmatic rocks or low-grade regionally metamorphosed metasediments (Veblen and Ribbe, 1982; Deer et al., 1992). Thus, chemical analysis of detrital blue amphibole is necessary to testify erosion of HP metamorphic blueschist facies rocks.

Blue sodic amphibole from sandstones of the BF are mostly glaucophane and Fe-glaucophane, although a few grains are crossite (Fig. 13). The high amount (~50%) of Fe-glaucophane is consistent throughout the mineral analyses of four samples and is unusual for presently exposed HP rocks of the Penninic unit (e.g., Oberhänsli, 1978, 1986; Philipp, 1982). Analyses of blue amphibole from sandstones of the TLF-succession show comparable composition but maximum Fe^{2+}# are lower (Fig. 13). These data support those of Winkler (1988) and prove the erosion of HP glaucophane-bearing rocks in the northwestern provenance area during, at least, Albian to Coniacian time.

Blue sodic amphibole in sandstones of the RF is extremely rare and displays a contrasting chemical composition: Fe^{2+}# are relatively low (<0.4) and Fe^{3+}# range from 0.2 to 0.8. Four out of eleven grains are Mg-riebeckite, five are crossite, and only two grains are glaucophane (Fig. 13). There are two conclusions to draw: (1) the blue sodic amphiboles from the RF are derived from a different source rock (the southeastern provenance area), and (2) due to their scarcity and chemical composition these minerals give no evidence for the erosion of HP metamorphic source rocks.

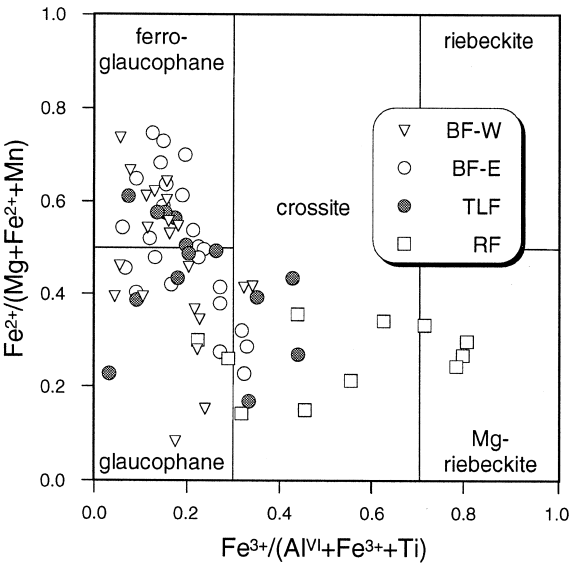

Fig. 13. Classification diagram of blue sodic amphibole (Leake, 1978). Minerals from the BF in the west (BF-W, $n = 20$), in the east (BF-E, $n = 24$), and from the TLF ($n = 14$) are glaucophane and ferro-glaucophane in composition. A few grains are crossite. Blue amphiboles from the RF ($n = 11$) are very rare and mostly crossite and Mg-riebeckite in composition.

8.1.2. Green and brown calcic amphibole

These minerals occur exclusively in sandstones of the RF (southeastern provenance, see Sections 3 and 6). They are Mg-rich ($Mg/(Mg + Fe^{2+}) > 0.5$) calcic amphiboles according to the classification scheme of Leake (1978). Green varieties are mostly actinolite or actinolitic hornblende, two grains are tremolite/tremolitic hornblende and two other grains are Mg-hornblende (Fig. 14). Brown varieties are tschermakitic, edenitic, Mg-hastingsitic and pargasitic hornblende, Mg-hornblende, pargasite and one grain of Ti-rich kaersutite. The green calcic amphiboles are most probably derived from very low- to low-grade metamorphic, e.g., greenschist facies rocks of basaltic composition. High Mg-actinolite and tremolite/tremolitic hornblende may also originate from low-grade regionally metamorphosed ultrabasic rocks (Deer et al., 1992). The brown calcic amphiboles are most probably derived from ultra-

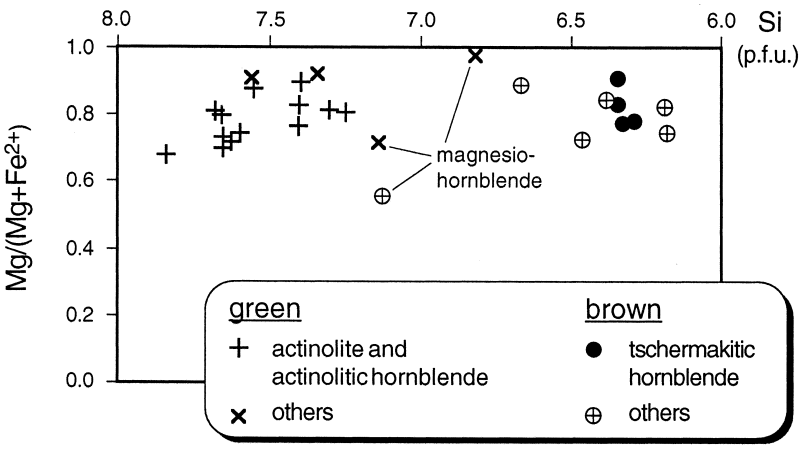

Fig. 14. Amphibole classification diagram according to Leake (1978). All grains are from RF sandstones ($n = 27$). Green varieties are actinolite and actinolitic hornblende. Others comprise magnesio-hornblende and two grains with Mg# >0.9 are tremolite and tremolitic hornblende. Brown varieties are tschermakitic hornblende, others comprise magnesio-hornblende and (due to contrasting Na, Fe^{3+} and Ti concentrations) pargasite, kaersutite as well as edenitic, Mg-hastingsitic and pargasitic hornblende.

basic to basic/intermediate magmatic rocks (von Eynatten, 1996). Schweigl and Neubauer (1997) recently reported augite from sandstones of the RF supporting a provenance from ultrabasic to intermediate magmatic source rocks.

8.2. White mica

White mica is a common detrital mineral phase in sandstones, especially in those derived from metamorphic source rocks (Pettijohn et al., 1987). In this study white mica is restricted to the di-octahedral varieties muscovite and phengite. Phengitic mica results from the coupled substitution of Si + (Mg, Fe^{2+}) for 2 Al and can be described as a continuous solid solution between the minerals muscovite and Al-celadonite. Ideal muscovite has a Si content of 3.0 per formula unit (p.f.u.; calculated on eleven oxygens). White di-octahedral K-mica with Si content considerably higher than 3.0 p.f.u. is termed phengitic mica. Ideal phengite has Si = 3.5 p.f.u. and (Mg, Fe) = 0.5 p.f.u. (Deer et al., 1992). The

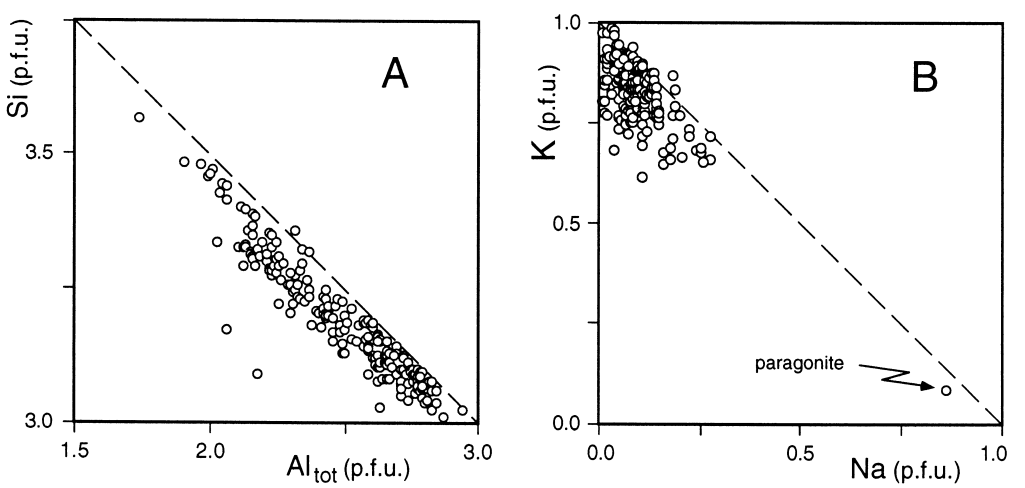

Fig. 15. Chemistry of the analyzed white mica ($n = 202$) grains illustrated in the Si vs. Al_{tot} (A) and K vs. Na (B) diagrams. The white K-micas are muscovite to phengite in composition, one single grain is a paragonite.

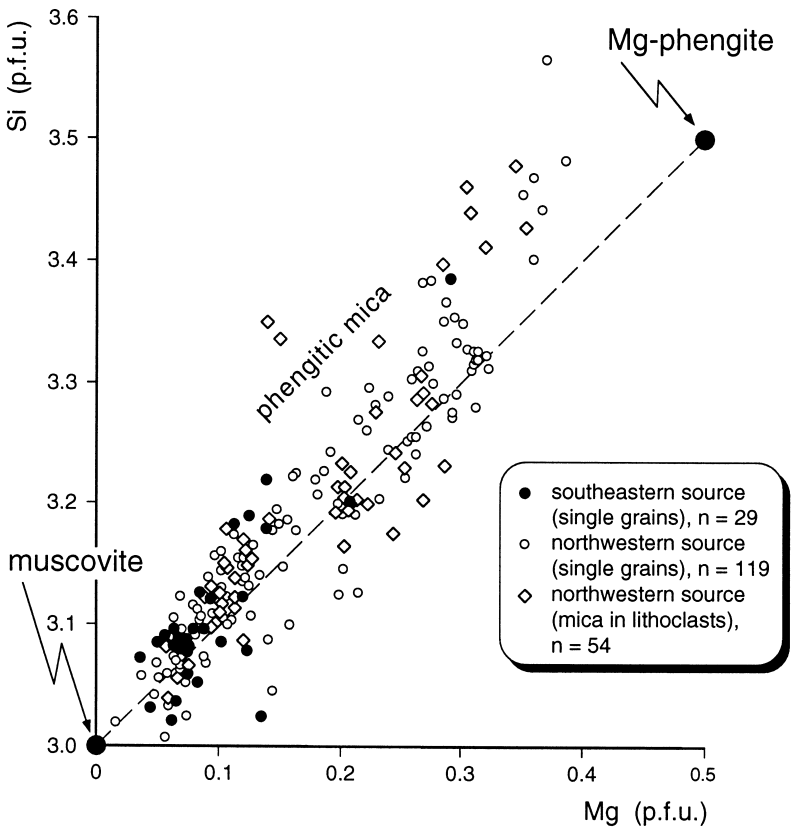

Fig. 16. Chemical composition of micas from the northwestern and the southeastern source area plotted in the Si vs. Mg diagram. Stippled line indicates 1 : 1 substitution of Si and Mg (replacing 2 Al). See text for explanation.

degree of substitution of Si + (Mg, Fe) largely depends on pressure during metamorphism. Mg-rich phengitic mica is indicative for metamorphic source rocks affected by relatively high-pressure and relatively low-temperature metamorphic conditions (e.g., Massonne and Schreyer, 1987).

The chemistry of individual mica grains (n = 202) is illustrated in the Si vs. Al(tot) and K vs. Na diagrams (Fig. 15A). Si content varies within a range from 3.0 to 3.4 p.f.u. with some grains displaying a higher celadonite component up to 3.57 Si p.f.u.. The correlation of the Si–Al exchange is very strong indicating low Fe^{3+} and Ti concentrations of the mica. All minerals are K-mica except one single grain of paragonite composition (Fig. 15B). Si + Mg substitution follows the 1 : 1 ratio line, thus indicating phengitic mica with negligible Fe^{2+} concentration except micas with Si >3.35 p.f.u. where minor Fe^{2+} substitution occurs (Fig. 16).

Mica of southeastern provenance (29 grains from six samples) are muscovitic in composition with Si content ranging from 3.07 to 3.22 p.f.u., and one single grain yielding 3.39 Si p.f.u. (Fig. 16). Detrital mica of northwestern provenance covers the whole range from muscovite with 3.01 Si p.f.u. up to phengite with max. 3.57 Si p.f.u.. Phengitic mica with >3.3 Si p.f.u. point to formation of these minerals under HP metamorphic conditions (Massonne and Schreyer, 1987). This is in agreement with the occurrence of HP metamorphic (Fe-)glaucophane, which is also restricted to the northwestern source area. Mica within lithoclasts from conglomerates and breccias of northwestern provenance range in Si content from 3.04 to 3.48 Si p.f.u.. Those clasts with micas >3.3 Si p.f.u. are metasandstones or metasiltstones which contain muscovitic as well as phengitic mica. This implies that at least some of the detrital mica are recy-

cled from older (?Permo–Carboniferous) sedimentary rocks.

8.3. Garnet

Garnet-group minerals are common in heavy mineral spectra of siliciclastic sediments and are generally interpreted to indicate metamorphic source rocks (Mange and Maurer, 1991). Garnet may also occur in magmatic rocks (Deer et al., 1992). Most natural garnets belong to the solid solution series between almandine (alm, Fe^{2+}-endmember), pyrope (prp, Mg-endmember), grossular (grs, Ca-endmember) and spessartine (sps, Mn-endmember). Due to its large chemical variability, microprobe analysis of detrital garnet has proven to be particularly useful in provenance studies (Morton, 1985, 1987; Haughton and Farrow, 1989; Yokoyama et al., 1990; Tebbens et al., 1995).

Detrital garnet analyzed in this study is usually almandine-rich (>50% up to 88%). Pyrope and grossular components generally range from a few percent to 30% with maximum values of 46% and 44%, respectively (Fig. 17A). About half of the minerals show a spessartine component exceeding 5%. Garnet of such composition cannot be unambiguously assigned to a specific lithology because garnet chemistry strongly depends on paragenesis and the chemistry of coexisting mineral phases. Generally, Fe-rich garnet is common in barrow-type metasediments (e.g., garnet-mica schists). Garnet with higher contents (20% to 30%) of the Mg-endmember and the Ca-endmember may originate from amphibolite, blueschist-associated eclogite, or granulite. Garnet peridotites and associated eclogites can be excluded as possible source rocks due to the low (<50%) pyrope component (Coleman et al., 1965; Deer et al., 1992).

Loosely following an approach of Morton (1992) we have classified the garnets into three types: (1) type-I garnet is a solid solution between almandine and pyrope with <10% grossular; (2) type-II garnet is a solid solution between almandine and grossular with <10% pyrope; and (3) type-III garnet with pyrope and grossular both >10% (Fig. 17A). This classification is used to discriminate between different garnet populations from the two source areas. Garnets from the southeastern source area (RF and LF) are dominated by type-I garnet (Fig. 17B). Garnets from the northwestern source area (TLF and

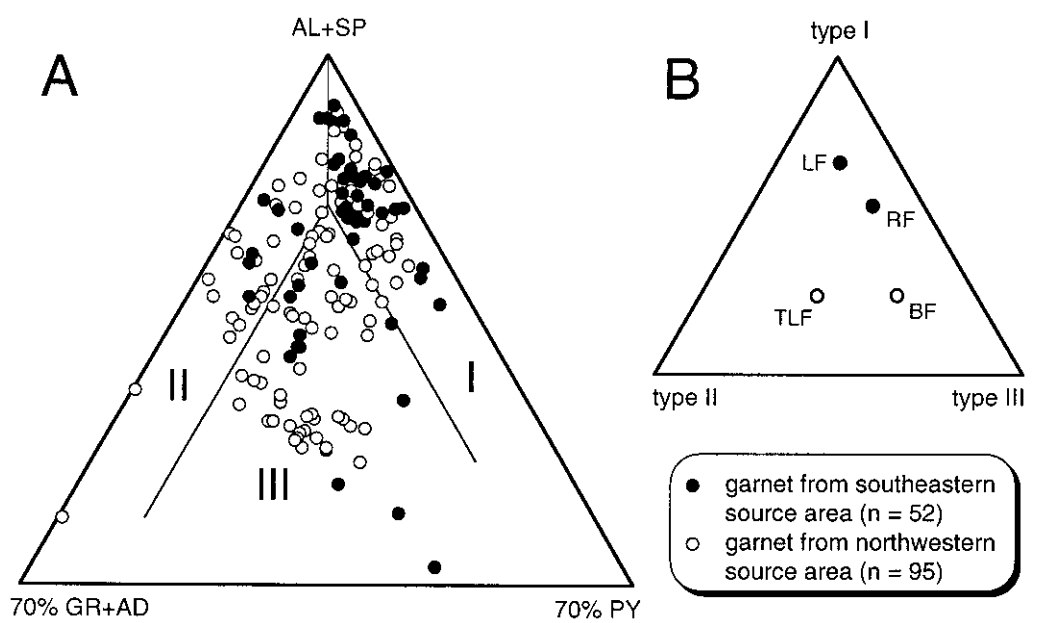

Fig. 17. Chemical composition of detrital garnet ($n = 147$). (A) Ternary diagram alm+sps – grs+adr – prp displaying the composition of individual mineral grains and classification of the three garnet types. (B) Ternary diagram displaying the composition of individual garnet populations with respect to the garnet types.

BF) are dominated by type-III garnet and display a higher amount of type-II garnet compared to garnet of the southeastern source area. Garnet with a possible origin from amphibolite and blueschist-associated eclogite (e.g., alm 50%, grs 20–30%, prp 20–30%, see above and Fig. 17A) is restricted to sediments of northwestern provenance. Garnet chemistry underlines the discrimination between the northwestern and the southeastern source area based on heavy mineral analysis and amphibole and mica chemistry.

8.4. Tourmaline

Tourmaline shows a wide range in chemical composition making it a suitable mineral phase for discrimination purposes. Most of the naturally occurring tourmalines can be described by the two continuous solid solution series: elbaite (Al-/Li-endmember) — schorl (Fe-endmember) and schorl — dravite/uvite (Mg-endmember). Tourmalines with high concentrations of Al, Li, and Fe are common in granitoids and pegmatites, whereas those with higher concentrations of Mg are common in metasediments and metasomatic rocks. Tourmaline is very resistant to both chemical and mechanical abrasion and thus forms a common accessory mineral phase in sandstones (Mange and Maurer, 1991; Deer et al., 1992). The chemical investigation of detrital tourmaline significantly widens the use of tourmaline in provenance analysis (e.g., Morton, 1991; Henry and Dutrow, 1992; Götze and Blankenburg, 1994). To extract petrogenetic information on the source rocks from the chemistry of detrital tourmaline, we use the tourmaline composition versus rock type classification scheme of Henry and Guidotti (1985; Fig. 18).

The analyzed tourmalines were derived from the northwestern source area (TLF and BF samples). Most of them plot into the compositional fields 3, 4, and 5 (Fig. 18A) or 6 (Fig. 18B) of the classification scheme from Henry and Guidotti (1985) indicating Ca-poor metasedimentary source rocks of varying Al and Fe^{3+} concentrations. Less than 15% of the measured grains ($n = 35$) plot into field 2 (Li-poor granitoids and pegmatites) suggesting either a minor acidic magmatic source rock component or recycling of primarily granitoid-derived tourmaline from older sedimentary rocks. (Meta)sediment clasts from conglomerates of the TLF contain tourmaline of largely comparable composition (black dots in Fig. 18). This supports the interpretation that a significant amount of the detrital tourmaline is recycled from older (meta)sedimentary rocks of Variscan or post-Variscan (Permo–Carboniferous) age.

8.5. Chloritoid

Chloritoid is a common mineral phase in low- to medium-grade metapelites of various pressure conditions (Deer et al., 1992). It has similar stability to

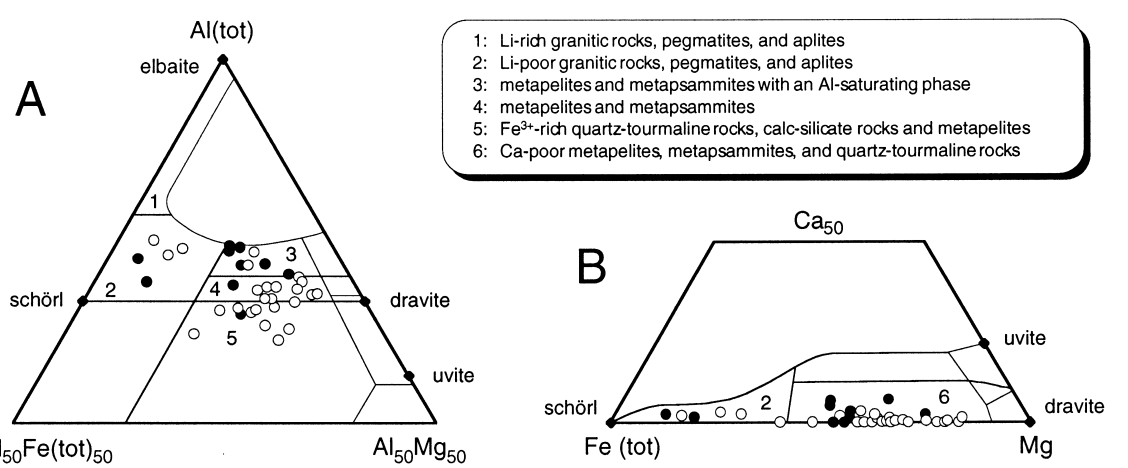

Fig. 18. Chemical composition of tourmaline from the northern provenance area (TLF and BF, $n = 35$). Diagrams from Henry and Guidotti (1985). Circles represent single tourmaline grains from heavy mineral separates, dots represent tourmaline within (meta)sediment clasts.

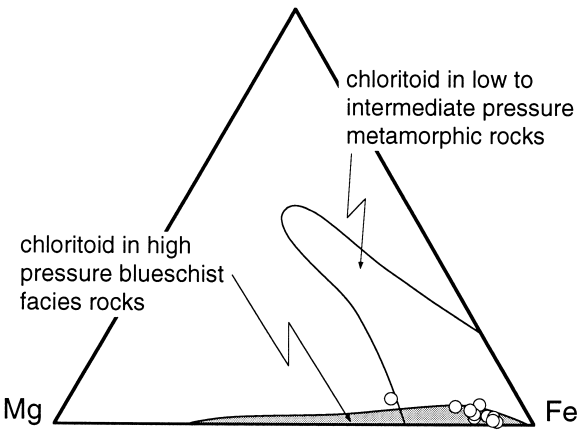

Fig. 19. Chemical composition of chloritoid from sandstones of the TLF and the BF ($n = 10$). Diagram after Chopin and Schreyer (1983).

garnet within the sedimentary cycle (Morton, 1985; Mange and Maurer, 1991). Variations in the chemical composition of chloritoid are generally defined by variations in the abundance of Fe, Mg, and Mn (Morton, 1991). Chloritoid from low- to medium-pressure barrow-type metapelites are usually rich in Fe and Mn, whereas chloritoid from HP blueschist-facies metapelites are rich in Fe and Mg (Fig. 19, Chopin and Schreyer, 1983). Chloritoid with Mg >50 mol.% is indicative for pressures of more than 15 to 18 kbar (Chopin, 1983).

Chloritoid analyses from sandstones of the northwestern provenance area ($n = 10$) have high Al concentrations (Al = 3.90 to 3.96 p.f.u.) indicating that nearly all of the measured total Fe is ferrous iron. The minerals display high Fe^{2+} concentrations (Fe# = Fe/(Fe + Mg + Mn) = 67 to 92 mol.%) and relatively low Mn (Mn = Mn/(Fe + Mg + Mn) = 1 to 6 mol.%) and Mg concentrations (Mg# = Mg/(Fe + Mg + Mn) = 7 to 14 mol.%, except one sample with Mg# = 27 mol.%). Nine of the analyses plot into the overlap of the fields for low/medium-pressure and HP metamorphic rocks (Fig. 19). Chloritoid of such composition is reported from blueschist facies rocks (e.g., Makanjuola and Howie, 1972; Chopin and Schreyer, 1983) but does not necessarily imply a HP source rock of these chloritoids. However, the correlation of glaucophane and chloritoid abundance in samples from the BF (see Section 6 and von Eynatten et al., 1997b) argues for an origin of these minerals in the same source area. Metamorphic source rocks which were affected by pressures in excess of 15–18 kbar (e.g., ultra-high-pressure (UHP) rocks) can be excluded due to the low Mg concentration of the chloritoid minerals.

9. Discussion

Previous studies on the provenance of some of the Cretaceous siliciclastic sediments of the Eastern Alps suggested two major source areas, but the provenance of LF and BF sediments still remained unclear (Section 3). Based on heavy mineral data (Section 6) we can integrate these two sedimentary successions into the concept of two source areas.

9.1. The northwestern source area

The northwestern source area was located at the transpressive plate margin between the Austroalpine microplate and the Penninic Ocean and was subject to erosion from the Aptian to the Coniacian/?Santonian (Sections 2 and 3). Light mineral data of sediments derived from this source (TLF and BF) indicate the erosion of ultrabasic rocks, low-grade metamorphic rocks, Permo–Carboniferous (meta)sediments, and Mesozoic carbonate rocks. The data suggest an overall increase of both Mesozoic carbonate rocks (especially dolomites) and ultrabasic rocks from the Albian (TLF) to the Coniacian/Santonian (BF, Fig. 8).

Heavy mineral data from TLF and BF samples indicate erosion of a continental crustal source (ZTR) and an oceanic crustal source (chrome spinel). Chrome spinel/ZTR ratios vary through time and space, but display a general increase towards younger BF samples (Fig. 10). The continental crustal source includes metamorphic rocks delivering garnet, epidote group minerals, chloritoid, and blue sodic amphibole. The latter two exclusively occur in sediments derived from the northwestern source area. This observation serves as a major discriminant between the two source areas.

The chemistry of blue sodic amphiboles prove a HP metamorphic origin of these grains. The data are strongly supported by the chemistry of detrital white mica which covers a wide compositional range from

muscovite to phengite. Thus we do have independent evidence from two mineral phases that indicate the erosion of HP metamorphic source rocks in the northwestern source area. Glaucophane and phengite data suggest a P–T range of the HP-rocks from 6 to 9 kbar at 300–400ºC (e.g., Massonne and Schreyer, 1987; Evans, 1990). Based on chloritoid chemistry and the relatively low pyrope content of the garnets metamorphic pressure in excess of 15–20 kbar can be excluded. Microprobe analyses of detrital tourmaline suggest mainly metasedimentary source rocks for these minerals. The low amount of tourmaline derived from granitoid rocks is in agreement with the low feldspar content of the sandstones.

Both light and heavy mineral data show an overall increase of the ultrabasic contribution for the stratigraphic younger BF compared with the TLF. The HP mineral phases correlate positively with the metamorphic lithoclasts and the stable heavy minerals ZTR (Section 7; von Eynatten et al., 1997b). Consequently, the HP minerals should be derived from HP rocks associated with continental crustal rocks. Assuming that the ultrabasic material (sepentinite, chrome spinel) in the sediments of northern provenance is derived from obducted Jurassic oceanic crust of the Penninic Ocean (e.g., Gaupp, 1983; Winkler, 1996), we conclude that glaucophane cannot be derived from blueschist facies rocks associated with this oceanic crustal source.

$^{40}Ar/^{39}Ar$ laserprobe dating of detrital white mica of the TLF and BF sedimentary successions yields exclusively Palaeozoic (mostly Carboniferous) ages indicating rapid cooling after the Variscan orogeny of the Palaeozoic basement of the Alps (von Eynatten et al., 1996). Phengite-rich samples yield Early Carboniferous ages indicating cooling after HP metamorphism associated with the final collision of Gondwana and Laurussia (Neubauer and von Raumer, 1993). No single Alpine age information can be inferred from our $^{40}Ar/^{39}Ar$ data. The narrow range in ages is in contrast with similar studies from the Himalayas where a composite geochronological structure of the hinterland is reflected by a wide range in detrital mica ages (Copeland and Harrison, 1990; Harrison et al., 1993; Najman et al., 1997). We conclude that Alpine metamorphic rocks were not exposed in the northwestern source area at the time of deposition of the analyzed sediments. This contradicts the model of Albian to Coniacian erosion of Lower Cretaceous HP-metamorphic rocks associated with subducted or obducted slabs of Penninic oceanic crust (Winkler and Bernoulli, 1986; Winkler, 1996).

9.2. The southeastern source area

This source area was located at the southeastern margin of the Austroalpine microplate including the Vardar/Meliata suture zone and was subject to erosion from the ?Berriasian/Valanginian to the uppermost Albian/?Cenomanian (Sections 2 and 3). Light mineral data of sediments derived from this source (RF and LF) indicate the erosion of Mesozoic carbonate rocks, ultrabasic rocks, and metamorphic/metasedimentary rocks. The light mineral data suggest a lower contribution of the ultrabasic source for LF sediments (Fig. 8) but this is contrasted by the heavy mineral data.

Heavy mineral spectra of both RF and LF samples are dominated by chrome spinel except for a few RF spectra which are dominated by green calcic amphibole. This implies a high contribution from the Vardar/Meliata oceanic suture zone. The relatively high maturity of LF sandstones (low D/Q_m rations, Fig. 8) is most probably responsible for the low concentration of mechanically unstable serpentinite fragments despite a high concentration of chrome spinel (see above). Metamorphic and (meta)sedimentary rocks are documented by ZTR minerals, green calcic amphibole, and garnet.

In the southeastern source area HP rocks were not exposed during the time documented by the analyzed sedimentary rocks. Blue sodic amphibole that rarely occur in RF sandstones are different in composition (mostly Mg-riebeckite and high-Fe^{3+}-crossite, Fig. 13) and do not prove the existence of HP metamorphic rocks in the southeastern provenance area. This is consistent with mica chemistry which reveals solely muscovitic compositions in both RF and LF samples. The absence of blue amphibole in sandstones from the LF cannot be explained by intrastratal solution because this process is not capable of changing mica chemistry from phengite to muscovite (see also Section 6).

Garnet composition provides a further tool for discrimination between the two source areas. Gar-

nets from the southeastern source are dominated by type-I garnets (alm ≫ prp > 10% > grs), whereas garnets from the northwestern source are dominated by type-III garnets (alm > prp ≈ grs > 10; Fig. 17). Type-I garnet is most probably derived from regionally metamorphosed metasedimentary rocks.

A significant feature of the heavy mineral spectra of the RF sandstones are green and to a minor extent brown calcic amphiboles. The former indicate erosion of very low- to low-grade metamorphic rocks of basaltic composition, whereas the latter indicate erosion of ultrabasic to intermediate magmatic rocks (Section 8.1.2). This possible magmatic source was most probably associated with the ultrabasic rocks (see also Schweigl and Neubauer, 1997). The stratigraphic younger LF sediments do not reflect this magmatic source. This may be due to either the higher maturity of the LF sandstones (see above) or a change in the source area through time.

9.3. Model of the tectono-sedimentary evolution

Several models of Alpine orogeny suggest a continuous southward subduction of Penninic oceanic crust below the Adriatic plate (including Austroalpine and Southalpine units, see Fig. 2) which led to HP metamorphism already in the Early Cretaceous (e.g., Winkler and Bernoulli, 1986; Stampfli, 1993; Wagreich, 1995). These models are in contradiction to (1) the almost complete absence of volcanism which should be expected if subduction lasted from the Early Cretaceous to the early Tertiary, (2) the occurrence of 100-Ma basanitic dikes/sills within the NCA which are derived from a subcontinental mantle source without any chemical or isotopic influence of a subducted plate (Trommsdorff et al., 1990), (3) the generally Tertiary age of Penninic HP rocks except for some scattered and doubtful Cretaceous data (see reviews in von Blanckenburg and Davies, 1995; Froitzheim et al., 1996), and (4) they do not take into account the Variscan age of the detrital HP minerals in the Cretaceous sediments (von Eynatten et al., 1996). The Penninic Ocean was a small (some hundreds of kilometer, e.g., Stampfli, 1993) ocean basin with a short phase of Middle/Upper Jurassic rifting and a tectonic control by transform faults (Kelts, 1981; Weissert and Bernoulli, 1985). This implies a relatively warm oceanic crust and a rough ocean floor topography at the time of onset of convergence. Convergence was oblique (e.g., Pfiffner, 1992) and resulted in a dextral transpressive stress regime at the former passive Austroalpine–Penninic plate margin. The plate margin was extensively fragmented due to Jurassic rifting (Eberli, 1988). This zone of weakness most probably accommodates both compressional and strike-slip movements. In such a scenario we do not expect the development of a large uniform Benioff zone. More likely is the formation of a transpressive plate margin controlled by both strike-slip faulting and thrusting/accretion.

Sedimentation models for the analyzed sediments suggest relatively small basins with moderately deep water conditions which developed parallel to prograding thrust fronts (e.g., Faupl and Tollmann, 1979; Gaupp, 1982). Characteristic features are gravitational mass flow deposits, rapid lateral facies changes, and a punctuated transversal sediment input from local fault scarps and submarine fans which may be diverted into longitudinal submarine lobes. The generally low maturity of the sedimentary rocks is typical for such environments. A high gradient source area is required due to low weathering indices despite a generally humid Cretaceous climate (Section 5.3). The sedimentological and petrographic data are consistent with deposition of the analyzed sedimentary rocks within piggyback basins (cf. Ori and Friend, 1984).

We suggest a modified tectono-sedimentary model of the Cretaceous (Valanginian to Coniacian) evolution in the Austroalpine unit. This model is based on (1) an onset of subduction of the Penninic Ocean no earlier than Late Cretaceous, (2) deposition of the analyzed sedimentary rocks within piggyback basins, and (3) a reconstruction of provenance as proposed in this study. The model may be subdivided into three stages (Fig. 20):

(A) Valanginian/Hauterivian: the Vardar/Meliata Ocean to the southeast of the Austroalpine is already closed and ultrabasic rocks of that suture zone were thrust together with continental crustal units of the Tisza block and/or the Southalpine onto the southeastern margin of the Austroalpine (see also Neubauer, 1994; Froitzheim et al., 1996). Together with Juvavic nappes these rocks formed an initial nappe pile within the Eastern Alps which acted as the source area for the Rossfeld Formation (RF).

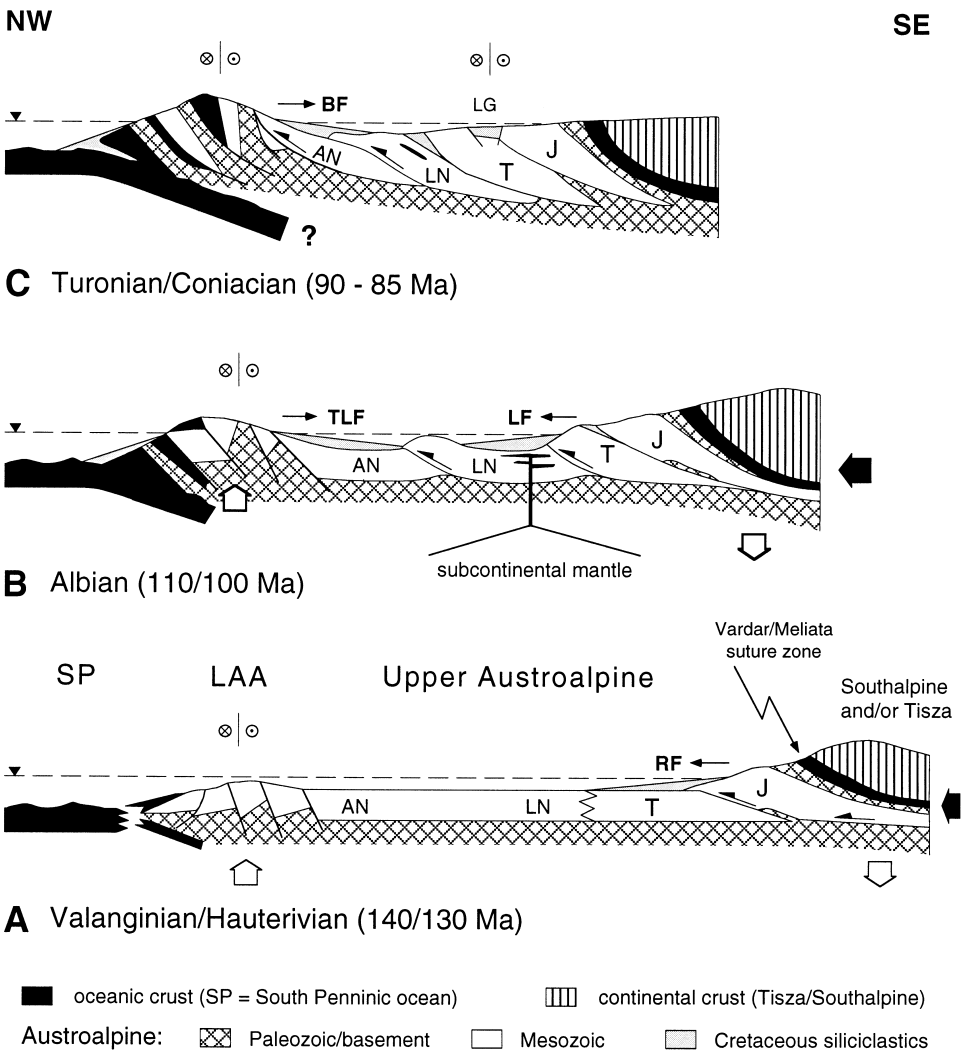

Fig. 20. Tectono-sedimentary model of the Valanginian to Coniacian evolution of the Austroalpine. See text for explanation. *AN* = Allgäu nappe (compare Fig. 4), *BF* = Branderfleck Formation, *J* = Juvavic nappes, *LAA* = Lower Austroalpine, *LF* = Lech Formation, *LG* = Lower Gosau Group, *LN* = Lechtal nappe, *RF* = Rossfeld Formation, *T* = Tirolic nappes, *TLF* = Tannheim and Losenstein Formations.

The transpressive plate margin at the northwestern tip of the Austroalpine (see above) experienced initial compression and resulting uplift most probably by reactivation of older passive margin faults. First slices of Penninic oceanic crust may be obducted or accreted.

(B) Albian: the orogenic wedge has prograded northwestward and constituted the source area for the sediments of the Lech Formation (LF) which were delivered from the southeast into the sedimentation area of the Lechtal nappe (LN). Basanitic dikes/sills within the Lechtal nappe indicate a subcontinental mantle below the NCA at that time. At the northwestern transpressive plate margin a new source area emerged due to the increased crustal shortening. Uplift of this source area is documented by a fission track peak age of detrital zircon derived from that source area at 120 ± 5 Ma (von Eynatten et al., 1997a). This antiform constitutes the catchment area for the sediments of the Aptian/Albian Tannheim

and Losenstein Formations (TLF). It is composed of Variscan low-grade metamorphic rocks including HP rocks, Palaeozoic (meta)sediments, Mesozoic carbonate rocks and slices of obducted Penninic oceanic crust.

(C) Turonian/Coniacian: the southeastern source area is no longer active due to erosion and deactivation of the Vardar/Meliata suture zone. In the area of the Juvavic (J) and Tirolic (T) nappes transtensive collapse basins were formed (Lower Gosau Group (LG); Wagreich and Faupl, 1994). The transpressive antiform at the northwestern margin is still emerged above sea level and acts as the source area of the sediments of the Branderfleck Formation (BF). Its composition is comparable to that during the Albian but the contribution of the ultrabasic source has increased as indicated by both light and heavy mineral data. Sedimentation of the BF continues up to the Coniacian/?Santonian when the northwestern source area became largely deactivated.

10. Conclusions

(1) The sedimentary rocks of the TLF and the BF are derived from a source area located to the northwest of the Upper Austroalpine in a Lower Austroalpine position near the transpressive plate margin to the Penninic Ocean. This source area was composed of Variscan low-grade metamorphic rocks including HP rocks, Permo–Carboniferous (meta)sediments, Mesozoic carbonate rocks and slices of obducted Penninic oceanic crust.

(2) The sedimentary rocks of the RF and the LF are both derived from a source area located at the southeastern margin of the Austroalpine including the Vardar/Meliata suture zone. This source area was composed of Palaeozoic metamorphic and sedimentary rocks, Mesozoic carbonate rocks and ultrabasic rocks derived from the suture zone of the Vardar/Meliata Ocean. No HP source rocks are documented by these sediments. A magmatic source associated with the ultrabasic rocks may be assumed for the time of deposition of the RF.

(3) The HP rocks of the northwestern source areas are associated with continental crustal rocks of the crystalline basement of the Alps and are Variscan in age (von Eynatten et al., 1996). Alpine HP metamorphism related to the subduction of Penninic oceanic crust is unlikely to occur earlier than in the Late Cretaceous. In combination with sedimentological and the new provenance data we establish a modified model of the Cretaceous tectono-sedimentary evolution of the Eastern Alps.

(4) An integrated approach to the provenance of siliciclastic rocks by combining several methods significantly enhances the potential of provenance analysis because each method is limited with respect to the posed questions. For example, light mineral analysis is useful for deducing climate and relief in the source area, but often fails in source area discrimination. Heavy mineral analysis is useful for provenance discrimination, but may fail in cases of an extensive diagenetic overprint or an extremely mature (stable) heavy mineral association. Chemical and geochronological analyses of single detrital grains are the most important tools to constrain petrology, tectonic setting, and the age of source rocks.

Acknowledgements

This study was financially supported by the Deutsche Forschungsgemeinschaft (grant Ga 457/1). We thank A. Kronz and B. Schulz-Dobrick (University of Mainz) for technical assistance with the microprobe. Fruitful discussions with Wolfgang Frisch, Roland Oberhänsli, and Jan Wijbrans improved our thoughts. We acknowledge careful and stimulating reviews by Andy Morton and Keith Sircombe.

References

Aitchison, J., 1982. The statistical analysis of compositional data. J. R. Statist. Soc. B 44, 139–177.

Arribas, J., Arribas, M.E., 1991. Petrographic evidence of different provenance in two alluvial fan systems (Paleogene of the northern Tajo Basin, Spain). In: Morton, A.C., Todd, S.P., Haughton, P.D.W. (Eds.), Developments in Sedimentary Provenance Studies. Geol. Soc. London, Spec. Publ. 57, 263–271.

Bangs Rooney, C., Basu, A., 1994. Provenance analysis of muddy sandstones. J. Sediment. Res. A 64, 2–7.

Channell, J.E.T., Horwath, F., 1976. The African/Adriatic promontory as a paleogeographical premise for Alpine orogeny and plate movements in the Carpatho-Balkan region. Tectonophysics 35, 71–101.

Channell, J.E.T., Brandner, R., Spieler, A., Stoner, J.S., 1992. Paleomagnetism and paleogeography of the Northern Calcareous Alps (Austria). Tectonics 11, 792–810.

Chopin, C., 1983. Magnesiochloritoid, a key-mineral for the petrogenesis of high-grade pelitic blueschists. Bull. Minéral. 106, 715–717.

Chopin, C., Schreyer, W., 1983. Magnesiocarpholite and magnesiochloritoid: two index minerals of pelitic blueschists and their preliminary phase relations in the model system MgO–Al_2O_3–SiO_2–H_2O. Am. J. Sci. 283, 72–96.

Coleman, R.G., Lee, D.E., Beatty, L.B., Brannock, W.W., 1965. Eclogites and eclogites: their differences and similarities. Bull. Geol. Soc. Am. 76, 483–508.

Copeland, P., Harrison, T.M., 1990. Episodic uplift in the Himalaya revealed by $^{40}Ar/^{39}Ar$ analysis of detrital K-feldspar and muscovite, Bengal fan. Geology 18, 354–357.

Cox, R., Lowe, D.R., 1996. Quantification of the effects of secondary matrix on the analysis of sandstone composition, and a petrographic–chemical technique for retrieving original framework grain modes of altered sandstones. J. Sediment. Res. 66, 548–558.

Darga, R., Weidich, K.F., 1986. Die Lackbach-Schichten, eine klastische Unterkreide-Serie in der Unkener Mulde (Nördliche Kalkalpen, Tirolikum). Mitt. Bayer. Staatssamml. Paläontol. Hist. Geol. 26, 93–112.

Decker, J., Helmold, K.P., 1985. The effect of grain size on detrital modes: a test of the Gazzi–Dickinson point-counting method — discussion. J. Sediment. Petrol. 55, 618–620.

Decker, K., Faupl, P., Müller, A., 1987. Synorogenic sedimentation on the Northern Calcareous Alps during the Early Cretaceous. In: Flügel, H.W., Faupl, P. (Eds.), Geodynamics of the Eastern Alps. Deuticke, Vienna, pp. 126–141.

Deer, W.A., Howie, R.A., Zussmann, J., 1992. An Introduction to the Rock-Forming Minerals, 2nd ed. Longman, Essex, 696 pp.

Dewey, J.F., Pitman, W.C., Ryan, W.B.F., Bonnin, J., 1973. Plate tectonics and the evolution of the Alpine system. Bull. Geol. Soc. Am. 84, 3137–3180.

Dickinson, W.R., 1970. Interpreting detrital modes of graywacke and arkose. J. Sediment. Petrol. 40, 695–707.

Dickinson, W.R., 1985. Interpreting provenance relations from detrital modes of sandstones. In: Zuffa, G.G. (Ed.), Provenance of Arenites. Reidel, Dordrecht, pp. 333–361.

Dickinson, W.R., Suczek, C.A., 1979. Plate tectonics and sandstone compositions. Bull. Am. Assoc. Pet. Geol. 63, 2164–2182.

Eberli, G.P., 1988. The evolution of the southern continental margin of the Jurassic Tethys Ocean as recorded in the Allgäu Formation of the Austroalpine Nappes of Graubünden (Switzerland). Eclogae Geol. Helv. 81, 175–214.

Evans, B.W., 1990. Phase relations of epidote-blueschists. Lithos 25, 3–23.

Faupl, P., Tollmann, A., 1979. Die Roßfeldschichten: ein Beispiel für Sedimentation im Bereich einer tektonisch aktiven Tiefseerinne aus der kalkalpinen Unterkreide. Geol. Rundsch. 68, 93–120.

Faupl, P., Wagreich, M., 1992. Cretaceous flysch and pelagic sequences of the Eastern Alps: correlations, heavy minerals, and paleogeographic implications. Cretaceous Res. 13, 387–403.

Flügel, E., Flügel-Kahler, E., 1992. Phanerozoic reef evolution: basic questions and data base. Facies 26, 167–277.

Folk, R.L., 1980. Petrology of Sedimentary Rocks. Hemphill, Austin, TX, 182 pp.

Francis, J.E., Frakes, L.A., 1993. Cretaceous climates. Sedimentol. Rev. 1, 17–30.

Frisch, W., 1979. Tectonic progadation and plate tectonic evolution of the Alps. Tectonophysics 60, 121–139.

Froitzheim, N., Schmid, S.M., Frey, M., 1996. Mesozoic paleogeography and the timing of eclogite-facies metamorphism in the Alps: a working hypothesis. Eclogae Geol. Helv. 89, 81–110.

Ganssloser, M., Theye, T., Wachendorf, H., 1996. Detrital glaucophane in graywackes of the Rhenohercynian Harz mountains and the geodynamic implications. Geol. Rundsch. 85, 755–760.

Garzanti, E., 1991. Non-carbonate intrabasinal grains in arenites: their recognition, significance, and relationship to eustatic cycles and tectonic setting. J. Sediment. Petrol. 61, 959–975.

Gaupp, R., 1982. Sedimentationsgeschichte und Paläotektonik der kalkalpinen Mittelkreide (Allgäu, Tirol, Vorarlberg). Zitteliana 8, 33–72.

Gaupp, R., 1983. Die paläogeographische Bedeutung der Konglomerate in den Losensteiner Schichten (Alb, Nördliche Kalkalpen). Zitteliana 10, 155–171.

Gaupp, R., Batten, D.J., 1985. Maturation of organic matter in Cretaceous strata of the Northern Calcareous Alps. Neues Jahrb. Geol. Paläontol. Monatsh. 1985, 157–175.

Götze, J., Blankenburg, H.-J., 1994. The genesis of the Hohenbocka quartz sand (Eastern Germany) — new results of mineralogical and geochemical investigations. Zentralbl. Geol. Paläontol. Teil 1 1992, 1217–1231.

Grantham, J.H., Velbel, M.A., 1988. The influence of climate and topography on rock-fragment abundance in modern fluvial sands of the southern Blue Ridge Mountains, North Carolina. J. Sediment. Petrol. 58, 219–227.

Harland, W.B., Armstrong, R.L., Cox, A.V., Craig, L.E., Smith, A.G., Smith, D.G., 1990. A Geologic Time Scale 1989. Cambridge University Press, Cambridge, 263 pp.

Harrison, T.M., Copeland, P., Hall, S.A., Quade, J., Burner, S., Ojha, T.P., Kidd, W.S.F., 1993. Isotopic preservation of Himalayan/Tibetan uplift, denudation, and climatic histories of two molasse deposits. J. Geol. 101, 157–175.

Haughton, P.D.W., Farrow, C.M., 1989. Compositional variations in Lower Old Red Sandstone garnets from the Midland Valley of Scotland and the Anglo-Welsh Basin. Geol. Mag. 126, 373–396.

Henry, D.J., Dutrow, B.L., 1992. Tourmaline in a low grade clastic metasedimentary rock: an example of the petrogenetic potential of tourmaline. Contrib. Mineral. Petrol. 112, 203–218.

Henry, D.J., Guidotti, C.V., 1985. Tourmaline as a petrogenetic indicator mineral: an example from the staurolite-grade metapelites of NW Maine. Am. Mineral. 70, 1–15.

Huckriede, R., 1958. Die Kreideschiefer bei Kaisers und Holzgan in den Lechtaler Alpen (Apt, Unteres Cenoman). Verh. Geol. Bundesanst. (Wien) 1958, 71–86.

Ibbeken, H., Schleyer, R., 1991. Source and Sediment. Springer, Berlin, 286 pp.

Ingersoll, R.V., Bullard, T.F., Ford, R.L., Grimm, J.P., Pickle, J.D., Sares, S.W., 1984. The effect of grain size on detrital modes: a test of the Gazzi–Dickinson point-counting method. J. Sediment. Petrol. 54, 103–116.

Kelts, K., 1981. A comparison of some aspects of sedimentation and translational tectonics from the Gulf of California and the Mesozoic Tethys, Northern Penninic Margin. Eclogae Geol. Helv. 74, 317–338.

Krumm, H., Petschick, R., Wolf, M., 1988. From diagenesis to anchimetamorphism, upper Austroalpine sedimentary cover in Bavaria and Tyrol. Geodin. Acta 2, 33–47.

Leake, B.E., 1978. Nomenclature of amphiboles. Can. Mineral. 16, 501–520.

Löcsei, J., 1974. Die geröllführende mittlere Kreide der östlichen Kalkvoralpen. Jahrb. Geol. Bundesanst. Wien 117, 17–54.

Mack, G.H., 1984. Exceptions to the relationship between plate tectonics and sandstone composition. J. Sediment. Petrol. 54, 212–220.

Makanjuola, A.A., Howie, R.A., 1972. The mineralogy of the glaucophane schists and associated rocks from Ile de Croix, Brittany, France. Contrib. Mineral. Petrol. 35, 83–118.

Mange, M.A., Maurer, H.F.W., 1991. Schwerminerale in Farbe. Enke, Stuttgart, 148 pp.

Mange-Rajetzky, M.A., 1981. Detrital blue sodic amphibole in Recent sediments, southern coast, Turkey. J. Geol. Soc. London 138, 83–92.

Mange-Rajetzky, M.A., Oberhänsli, R., 1982. Detrital lawsonite and blue sodic amphibole in the Molasse of Savoy, France and their significance in assessing Alpine evolution. Schweiz. Mineral. Petrogr. Mitt. 62, 415–436.

Massonne, H.-J., Schreyer, W., 1987. Phengite geobarometry based on the limiting assemblage with K-feldspar, phlogopite, and quartz. Contrib. Mineral. Petrol. 96, 212–224.

McBride, E.F., 1963. A classification of common sandstones. J. Sediment. Petrol. 33, 664–669.

Misík, M., Sykora, M., 1981. Der pieninische exotische Rücken, rekonstruiert aus Geröllen karbonatischer Gesteine kretazischer Konglomerate der Klippenzone und der Manín-Einheit. Západné Karpaty, Sér. Geológia 7, 91–111.

Morton, A.C., 1985. Heavy minerals in provenance studies. In: Zuffa, G.G. (Ed.), Provenance of Arenites. Reidel, Dordrecht, pp. 249–277.

Morton, A.C., 1987. Influences of provenance and diagenesis on detrital garnet suites in the Forties sandstone, Paleocene, central North Sea. J. Sediment. Petrol. 57, 1027–1032.

Morton, A.C., 1991. Geochemical studies of detrital heavy minerals and their application to provenance research. In: Morton, A.C., Todd, S.P., Haughton, P.D.W. (Eds.), Developments in Sedimentary Provenance Studies. Geol. Soc. London, Spec. Publ. 57, 31–45.

Morton, A.C., 1992. Provenance of Brent Group sandstones: heavy mineral constraints. In: Morton, A.C., Haszeldine, R.S., Giles, M.R., Brown, S. (Eds.), Geology of the Brent Group. Geol. Soc. London, Spec. Publ. 61, 227–244.

Morton, A.C., Hallsworth, C., 1994. Identifying provenance-specific features of detrital heavy mineral assemblages in sandstones. Sediment. Geol. 90, 241–256.

Najman, Y.M.R., Pringle, M.S., Johnson, M.R.W., Robertson, A.H.F., Wijbrans, J.R., 1997. Laser $^{40}Ar/^{39}Ar$ dating of single detrital muscovite grains from early foreland-basin deposits in India: implications for early Himalayan evolution. Geology 25, 535–538.

Neubauer, F., 1987. The Gurktal thrust system within the Austroalpine region — some structural and geometrical aspects. In: Flügel, H.W., Faupl, P. (Eds.), Geodynamics of the Eastern Alps. Deuticke, Vienna, pp. 226–236.

Neubauer, F., 1994. Kontinentkollision in den Ostalpen. Geowissenschaften 12, 136–140.

Neubauer, F., von Raumer, J.F., 1993. The Alpine basement — linkage between Variscides and East-Mediterranean mountain belts. In: von Raumer, J.F., Neubauer, F. (Eds.), Pre-Mesozoic Geology in the Alps. Springer, Berlin, pp. 641–663.

Oberhänsli, R., 1978. Chemische Untersuchungen an Glaukophan-führenden basischen Gesteinen aus den Bündnerschiefern Graubündens. Schweiz. Mineral. Petrogr. Mitt. 58, 139–156.

Oberhänsli, R., 1986. Blue amphiboles in metamorphosed Mesozoic mafic rocks from the Central Alps. Geol. Soc. Am. Mem. 164, 239–247.

Ori, G.G., Friend, P.F., 1984. Sedimentary basins formed and carried piggyback on active thrust sheets. Geology 12, 475–478.

Pettijohn, F.J., Potter, P.E., Siever, R., 1987. Sand and Sandstone. Springer, New York, 553 pp.

Pfiffner, A., 1992. Alpine orogeny. In: Blundell, D., Freeman, R., Mueller, S. (Eds.), The European Geotraverse. Cambridge University Press, Cambridge, pp. 180–190.

Philipp, R., 1982. Die Alkaliamphibole der Platta-Decke zwischen Silsersee und Lunghinpass (Graubünden). Schweiz. Mineral. Petrogr. Mitt. 62, 437–455.

Pober, E., Faupl, P., 1988. The chemistry of detrital chromian spinels and its implications for the geodynamic evolution of the Eastern Alps. Geol. Rundsch. 77, 641–670.

Pouchou, J.L., Pichoir, F., 1984. A new model for quantitative X-ray microanalysis, Part I. Application to the analysis of homogeneous samples. Rech. Aérospatiale 3, 13–38.

Schweigl, J., Neubauer, F., 1997. New structural, sedimentological and geochemical data on the Cretaceous geodynamics of the central Northern Calcareous Alps (Eastern Alps). Zentralbl. Geol. Paläontol. Teil 1 1996, 329–343.

Stampfli, G.M., 1993. Le Briançonnais, terrain exotique dans les Alpes? Eclogae Geol. Helv. 86, 1–45.

Tebbens, L.A., Kroonenberg, S.B., van der Berg, M.W., 1995. Compositional variation of detrital garnets in Quaternary Rhine, Meuse and Baltic River sediments in the Netherlands. Geol. Mijnbouw 74, 213–224.

Till, A.B., 1992. Detrital blueschist-facies metamorphic mineral assemblages in Early Cretaceous sediments of the foreland

basin of the Brooks Range, Alaska, and implications for orogenic evolution. Tectonics 11, 1207–1223.

Trommsdorff, V., Dietrich, V., Flisch, M., Stille, P., Ulmer, P., 1990. Mid-Cretaceous, primitive alkaline magmatism in the Northern Calcareous Alps: significance for Austroalpine geodynamics. Geol. Runddsch. 79, 85–97.

Van der Plas, L., Tobi, A.C., 1965. A chart for judging the reliability of point counting results. Am. J. Sci. 263, 87–90.

Veblen, D.R., Ribbe, P.H., 1982. Amphiboles: Petrology and Experimental Phase Relations. Miner. Soc. Am., Rev. Mineral. 9B, 390 pp.

Von Blanckenburg, F., Davies, J.H., 1995. Slab breakoff: a model for syncollisional magmatism and tectonics in the Alps. Tectonics 14, 120–131.

Von Eynatten, H., 1996. Provenanzanalyse kretazischer Siliziklastika aus den Nördlichen Kalkalpen: Petrographie, Mineralchemie und Geochronologie des frühalpidisch umgelagerten Detritus. Doctoral Thesis, University of Mainz, 145 pp. (unpubl.).

Von Eynatten, H., Gaupp, R., Wijbrans, J.R., 1996. $^{40}Ar/^{39}Ar$ laser-probe dating of detrital white micas from Cretaceous sedimentary rocks of the Eastern Alps: evidence for Variscan high-pressure metamorphism and implications for Alpine orogeny. Geology 24, 691–694.

Von Eynatten, H., Gaupp, R., Wijbrans, J.R., Brix, M., 1997a. Provenance of Cretaceous synorogenic sediments in the Eastern Alps: an integrated approach using mineralogical, geochemical, and geochronological methods. Terra Nova 9, Abstr. Suppl. 1, 593.

Von Eynatten, H., Gaupp, R., Wijbrans, J.R., 1997b. $^{40}Ar/^{39}Ar$ laser-probe dating of detrital white micas from Cretaceous sedimentary rocks of the Eastern Alps: evidence for Variscan high-pressure metamorphism and implications for Alpine orogeny. Comment and Reply. Geology 25, 765–767.

Wagreich, M., 1995. Subduction tectonic erosion and Late Cretaceous subsidence along the northern Austroalpine margin (Eastern Alps, Austria). Tectonophysics 242, 63–78.

Wagreich, M., Faupl, P., 1994. Palaeogeography and geodynamic evolution of the Gosau Group of the Northern Calcareous Alps (Late Cretaceous, Eastern Alps, Austria). Palaeogeogr., Palaeoclimatol., Palaeoecol. 110, 235–254.

Weidich, K.F., 1984. Über die Beziehungen des ‘Cenomans’ zur Gosau in den Nördlichen Kalkalpen und ihre Auswirkungen auf die paläogeographischen und tektonischen Vorstellungen. Geol. Rundsch. 73, 517–566.

Weidich, K.F., 1985. Stratigraphie der Branderfleck-Schichten (Untercenoman–Untercampan) in den Bayerischen Kalkalpen. Schriftenr. Erdwiss. Komm. 7, 221–261.

Weissert, H.J., Bernoulli, D., 1985. A transform margin in the Mesozoic Tethys: evidence from the Swiss Alps. Geol. Rundsch. 74, 665–679.

Weltje, G.J., 1994. Provenance and dispersal of sand-sized sediments. Geol. Ultraiectina 121, 1–208.

Winkler, W., 1988. Mid- to Early Late Cretaceous flysch and melange formations in the western part of the Eastern Alps. Palaeotectonic implications. Jahrb. Geol. Bundesanst. Wien 131, 341–389.

Winkler, W., 1996. The tectono-metamorphic evolution of the Cretaceous northern Adriatic margin as recorded by sedimentary series (western part of the Eastern Alps. Eclogae Geol. Helv. 89, 527–551.

Winkler, W., Bernoulli, D., 1986. Detrital high-pressure/low-temperature minerals in a late Turonian flysch sequence of the eastern Alps (western Austria): implications for early Alpine tectonics. Geology 14, 598–601.

Yokoyama, K., Amano, K., Taira, A., Saito, Y., 1990. Mineralogy of silts from the Bengal Fan. Proc. ODP, Sci. Results 116, 59–73.

Zacher, W., 1966. Die kalkalpinen Kreide-Ablagerungen in der Umgebung des Tannheimer Tales (Außerfern, Tirol). Mit einem mikropaläontologischen Beitrag von F. Bettenstaedt. Mitt. Bayer. Staatssamml. Paläontol. Hist. Geol. 6, 213–228.

Zimmerle, W., 1984. The geotectonic significance of detrital brown spinel in sediments. Mitt. Geol.-Paläontol. Inst. Univ. Hamburg 56, 337–360.

Zuffa, G.G., 1980. Hybrid arenites: their composition and classification. J. Sediment. Petrol. 50, 21–29.

Zuffa, G.G., 1985. Optical analyses of arenites: influence of methodology on compositional results. In: Zuffa, G.G. (Ed.), Provenance of Arenites. Reidel, Dordrecht, pp. 165–189.